Chem Soc Rev

ROYAL SOCIETY OF CHEMISTRY

REVIEW ARTICLE

View Article Online
View Journal | View Issue

Cite this: *Chem. Soc. Rev.*, 2021, **50**, 13346

A multifunctional 2D black phosphorene-based platform for improved photovoltaics

Meng Zhang, Gill M. Biesold and Zhiqun Lin *

As one of the latest additions to the 2D nanomaterials family, black phosphorene (BP, monolayer or few-layer black phosphorus) has gained much attention in various forms of solar cells. This is due largely to its intriguing semiconducting properties such as tunable direct bandgap (from 0.3 eV in the bulk to 2.0 eV in the monolayer), extremely high ambipolar carrier mobility, broad visible to infrared light absorption, *etc.* These appealing optoelectronic attributes make BP a multifunctional nanomaterial for use in solar cells *via* tailoring carrier dynamics, band energy alignment, and light harvesting, thereby promoting the rapid development of third-generation solar cells. Notably, in sharp contrast to the copious work on revealing the fundamental properties of BP, investigation into the utility of BP is comparatively less, particularly in the area of photovoltaics. Herein, we first identify and summarize an array of unique characteristics of BP that underpin its application in photovoltaics, aiming at providing inspiration to develop new designs and device architectures of photovoltaics. Subsequently, state-of-the-art synthetic routes (*i.e.*, top-down and bottom-up) to scalable BP production that facilitates its applications in optoelectronic materials and devices are outlined. Afterward, recent advances in a diverse set of BP-incorporated solar cells, where BP may impart electron and/or hole extraction and transport, function as a light absorber, provide dielectric screening for enhancing exciton dissociation, and modify the morphology of photoabsorbers, are discussed, including organic solar cells, dye-sensitized solar cells, heterojunction solar cells and perovskite solar cells. Finally, the challenges and opportunities in this rapidly evolving field are presented.

Received 6th September 2021

DOI: 10.1039/d1cs00847a

rsc.li/chem-soc-rev

1. Introduction

The past few decades have witnessed the exponentially growing interest in two-dimensional (2D) materials across a wide range of science and engineering disciplines owing to their unique structures and outstanding properties. Among the family of 2D nanomaterials, black phosphorene (BP, monolayer or few-layer black phosphorus) as one of the newest additions has gained significant attention due to its intrinsic semiconducting properties for use in optoelectronics and nanoelectronics.[1] BP was first exfoliated in early 2014 using a scotch-tape micro-cleavage method, a well-known approach for graphene isolation.[2] Although research into the potential applications of BP is at an early stage, tremendous efforts centered on investigating its fundamental properties have provided a

School of Materials Science and Engineering, Georgia Institute of Technology, Atlanta, GA 30332, USA. E-mail: zhiqun.lin@mse.gatech.edu

Meng Zhang

Dr Meng Zhang is a research scientist in Dr Zhiqun Lin's group at the School of Materials Science and Engineering, Georgia Institute of Technology. She received her PhD degree in Engineering Thermophysics from Zhejiang University, China, in 2016. Her research interests are centered on solar energy conversion and storage, including perovskite solar cells, CO_2 conversion and utilization, and advanced energy materials.

Gill M. Biesold

Gill M. Biesold is a PhD student in Materials Science and Engineering at Georgia Institute of Technology. He received his BS in Materials Science and Engineering from Clemson University in 2017. His current research is focused on the synthesis of colloidal semiconductor nanocrystals and their optoelectronic properties.

distinct recognition of BP in the 2D material community. BP was revealed to be an ambipolar semiconductor with a tunable direct bandgap (E_g) ranging from 0.3 eV in the bulk to 2.0 eV in the monolayer, thus perfectly bridging that of graphene ($E_g = 0$) and semiconducting transition metal dichalcogenides ($E_g >$ 1.57 eV).[3,4] Moreover, in contrast to other 2D materials, BP possesses not only strong in-plane anisotropy but also outstanding properties (*e.g.*, good carrier mobility, high current on/off ratio, and excellent thermoelectric properties).[1] In the latter context, few-layer BP-based field-effect transistors (FET) have been reported to demonstrate a current on/off ratio of 10^5 and a hole mobility of up to 1000 $cm^2\ V^{-1}\ s^{-1}$.[2] Notably, intriguing properties in conjunction with a unique 2D structure make BP an ideal candidate for application in many fields. To date, BP has been effectively utilized in transistors, batteries, supercapacitors, catalysis, and solar cells, clearly highlighting the significance and prospects of BP for energy and sustainability.

Solar cells are recognized as an extremely promising area for use of BP-based materials.[5,6] In recent years, the need for renewable and sustainable energy resources has greatly increased due to fossil fuel depletion. Solar cells, converting solar energy directly into electricity, have great potential to solve energy and environmental concerns at low cost. As the first-generation photovoltaics developed in the 1970s, Si-based solar cells face issues associated with expensive fabrication cost which limit their wide use.[7,8] Notably, the development of the second-generation photovoltaics (*i.e.* thin-film solar cells) is also plagued by the same issue.[7] Recently, as the third-generation photovoltaics, organic solar cells (OSCs), dye-sensitized solar cells (DSSCs), heterojunction solar cells (HJSCs) and perovskite solar cells (PSCs) have emerged as alternatives to Si-based solar cells. Among them, PSCs have received tremendous attention. Since the introduction of PSCs in 2009, their power conversion efficiency (PCE) has increased from 3.8% to 25.5% using solution-based deposition methods,[9] demonstrating their promising potential to rival commercial Si-based solar cells due to the high PCE and easy solution fabrication of PSCs.[10] It is worth noting that extensive efforts are centered on investigating the active layer, electrodes, and interlayers to improve the efficiency and stability of the third-generation photovoltaics needed for commercial applications. Specifically, PSCs experience low stability and scale-up efficiency.[10] On the other hand, OSCs, DSSCs and quantum dot-sensitized solar cells (QDSSCs) do not possess competitive PCE over Si-based solar cells.[9] Due to a set of intriguing semiconducting properties, 2D BP may operate in a multi-functional manner, including tailoring carrier dynamics, improving band energy alignment, enhancing light harvesting, *etc.*, in different categories of photovoltaics,[5] demonstrating its potential in advancing the third-generation photovoltaics.

In this review, the recent progress in capitalizing on extraordinary attributes of BP in various photovoltaics is discussed. First, a general overview of the structure and fundamental properties of BP is provided, and the application of BP in photovoltaics is highlighted. Subsequently, the current scalable synthetic routes to BP nanosheets and quantum dots that facilitate their implementation for use in optoelectronic materials and devices are summarized. Then, recent advances in a variety of BP-incorporated solar cells, including OSCs, DSSCs, HJSCs and PSCs, is assessed, where BP imparts electron and/or hole extraction and transport, light harvesting, and dielectric screening for enhancing exciton dissociation and modification of the photoabsorber morphology to improve device performance. Finally, challenges and opportunities that may enable advanced implementation of BP in photovoltaics are outlined. This review may guide future fundamental and applied research that capitalizes on the peculiar properties of BP for use in a rich variety of optoelectronic materials and devices.

Zhiqun Lin

Dr Zhiqun Lin is a professor at the School of Materials Science and Engineering, Georgia Institute of Technology. His research interests include solar energy conversion, photocatalysis, electrocatalysis, batteries, semiconductor organic–inorganic nanocomposites, multifunctional nanocrystals, conjugated polymers, block copolymers, hierarchical structure formation and assembly, and surface and interfacial properties.

2. An array of appealing properties of BP for use in photovoltaics

2.1. Crystal and atomic structure

Phosphorus is one of the most abundant elements on the earth and possesses four allotropes: white, red, violet, and black, all named according to their appearance. White phosphorus and red phosphorus, the two major allotropes, readily catch fire and are unstable in ambient air. Black phosphorus is the most thermodynamically stable and conductive allotrope. It was first discovered in 1914 *via* a high pressure (up to 1.2 GPa at 200 °C) transformation of white phosphorus.[11] Black phosphorus bulk crystals consist of stacked layer structures and have been termed phosphorene. The interlayer interactions between these stacking layers are comparable to van der Waals interactions, which can be easily broken to obtain monolayer or few-layer phosphorene (BP). The inherent properties of 2D nanostructures such as large specific surface area, in-plane confinement of electrons, and flexibility could have a substantial impact on photovoltaics in a host of occasions. Particularly, 2D materials are perfect candidates for interfacial application in solid-state solar cells. The formation of van der Waals heterostructures could modulate the band alignment, charge distribution, separation, and transport.

Structurally, monolayer BP consists of covalently bonded sp^3 hybridized phosphorus atoms. Each P atom is saturated, covalently bonded to three neighboring P atoms, and has one lone-pair of electrons. This bonding leads to a quadrangular pyramid structure resembling a puckered honeycomb (Fig. 1).[12] The puckered layer can be regarded as two parallel planes with the P atoms in each plane arranged along zigzag-like and armchair-like geometric edges. The lattice constants for the armchair and zigzag edges are 4.37 Å and 3.31 Å, respectively, and the dihedral angle and hinge angle have been measured to be 102° and 96°, respectively. The similarity in the distance of the adjacent P–P bond length (d_1 = 2.224 Å) and the connecting bond length (d_2 = 2.244 Å) can be ascribed to the covalent bonds derived from phosphorus 3p orbitals.[12] Few-layer BP forms from the stacking of BP monolayers *via* a weak interlayer interaction (20 meV atom^{-1}).[6] The sheet–sheet spacing between two BP layers is around 5.3 Å, which is greater than the interlayer spacing of graphene (3.4 Å). The relatively large spacing is due to its puckered structure, as well as the AB Bernal stacking of two BP layers in the unit cell.[6] The sp^3 orbital hybridization results in a highly asymmetric structure and unique in-plane anisotropic properties of BP. This anisotropy is significantly reflected in the effective masses and anisotropic behavior of electrons, photons, and phonons.[13,14] The anisotropy adds a new dimension to the properties of 2D BP-based materials and stimulates the development of angle-resolved photonics and electronics. The application of BP's anisotropy remains an unexplored area in photovoltaics and may stimulate the development of smart photovoltaic devices.

2.2. Electronic band structure

The electronic band structure of BP exhibits two significant characteristics: a layer-independent direct bandgap and layer-dependent bandgap value.[15] The consistent direct bandgap of BP differentiates it from most of the other 2D semiconductors (such as MoS_2 and WS_2) which present a gap at the *K* point and display an indirect-to-direct bandgap transition upon going from bulk to monolayer.[1,16] Notably, the band gap of BP remains direct at the *Γ* point of the Brillouin zone and is independent of the number of layers.[17] The bandgap of bulk BP is also direct, but it moves to the *Z* point of the Brillouin zone.[2] The constant direct bandgap of BP greatly expands its optoelectronic applications.

Another representative characteristic of BP is its thickness-dependent bandgap. The valence band maximum (VBM) and conduction band minimum (CBM) of BP are composed of a mixture of s and p orbitals (p_z-orbitals).[18–20] The variation in the magnitude of the band gap is due to the linear combination of these p_z orbitals with additional layers.[20,21] The effect of the number of BP layers on bandgap values has been widely investigated both theoretically and experimentally.[2,4,22,23] Though the exact magnitudes show a wide variation, the main trend reveals that BP's bandgap decreases with the increasing number of layers, accompanied by the concurrent splitting of the bands. Specifically, the bandgap of monolayer BP decreases from about 2.0 eV to 0.3 eV in the bulk form based on the calculations using the GW method in the G_0W_0 approximation, which is one of the most reliable first-principles electronic structure methods for bandgap determination.[16] Notably, these bandgap values are unique to BP and enable values unavailable for graphene and transition metal dichalcogenides (TMD), which makes BP particularly promising for various electronic devices (Fig. 2).[17] The band gap of BP has also been tuned with strain, external electrical field, rotation angles between BP sheets, functionalization, and doping.[24–26] BP exhibits an exceptional degree of tunability that has not been observed for other 2D layered semiconductors, which makes it unique for various applications.

To effectively utilize BP in photovoltaics, matching its energy levels with that of other components used in solar cells to

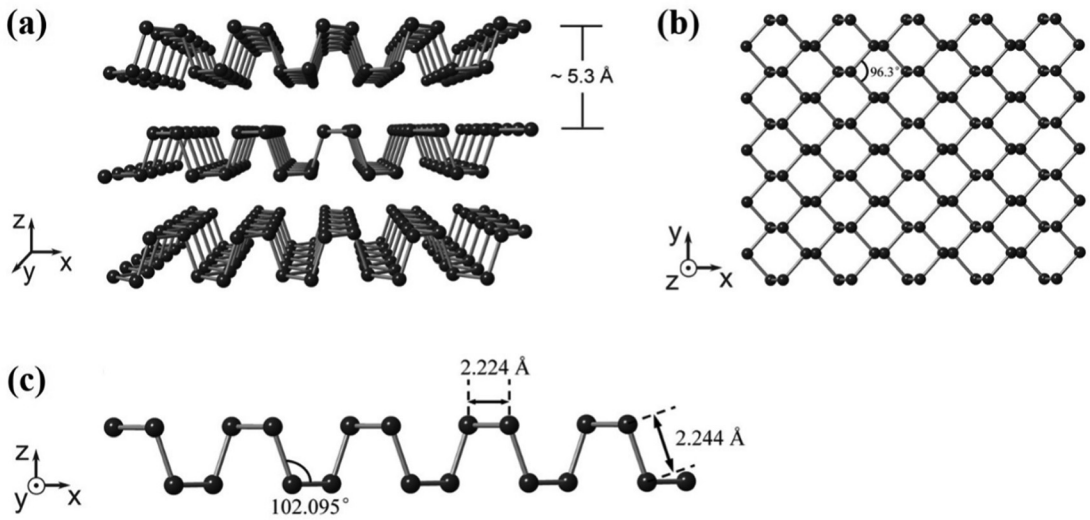

Fig. 1 Atomic structure of black phosphorene. (a) Bird's eye view, (b) top view and (c) side view. Reproduced with permission from ref. 12. Copyright 2015, The Royal Society of Chemistry. Note: *X* and *Y* axes correspond to the armchair and zigzag directions, respectively.

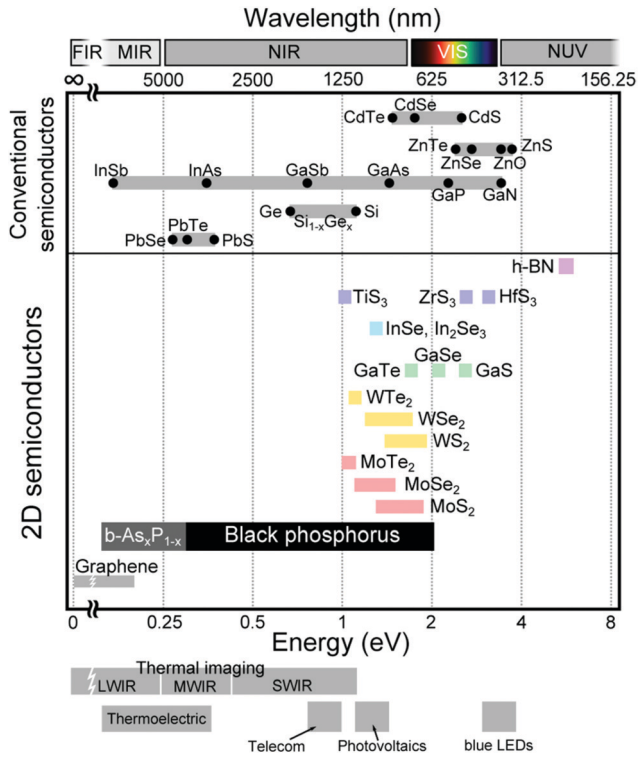

Fig. 2 Comparison of the band gap values for different 2D semiconductor materials. Reproduced with permission from ref. 17. Copyright 2015, American Chemical Society.

achieve a cascade band gap alignment is of great importance. Charge transfer processes must be energetically favorable in order to achieve high photovoltaic performance. The bandgap and energy levels of the BP (from 1 to 5 layers) are plotted and compared with the commonly used components in emerging solar cells, including PSCs, OSCs, and DSSCs (Fig. 3). Notably, the energy levels of few-layer BP are similar to those of various functional components in solar cells, including light absorbers, electron selective materials, and hole selective materials. This similarity in bandgap indicates the potential for BP to act as a multifunctional additive in photovoltaic applications. In addition to altering the thickness, functionalization and doping are other strategies that further enrich the toolbox in tailoring the bandgap of BP for various optoelectronic applications.

2.3. Charge transport

High carrier mobility, the core parameter for electron–hole transport, is one of the key prerequisites for materials in photovoltaic applications. Bulk BP demonstrates slight p-type conductivity with a positive Hall coefficient, but it exhibits high mobility for both electrons and holes. The carrier mobilities of bulk BP at room temperature are as high as 350 $cm^2 V^{-1} s^{-1}$ for holes and 220 $cm^2 V^{-1} s^{-1}$ for electrons.[28] These values can be further increased up to 1000 $cm^2 V^{-1} s^{-1}$ for thin BP nanosheets.[2] Typically, the charge mobility of BP increases with the increased thickness of up to about 10 nm in few-layer BP (apart from the monolayer).[29] The asymmetry and anisotropy of carrier mobility in few-layer BP are inversely related to the effective mass.[6] Since the effective masses of electrons and holes along the x direction are smaller than those along the y direction, the conductivity along the x direction (the armchair direction) is approximately one order of magnitude greater than that along the y direction.[6,30,31] However, it is different in BP monolayers. The effective masses of electrons (and holes) along the x and y directions are $0.17m_0$ ($0.15m_0$) and $1.1m_0$ ($6.35m_0$), respectively, in BP monolayers.[30] The electron mobility in the x direction (1140 $cm^2 V^{-1} s^{-1}$) is observed to be higher than that in the y direction (80 $cm^2 V^{-1} s^{-1}$). However,

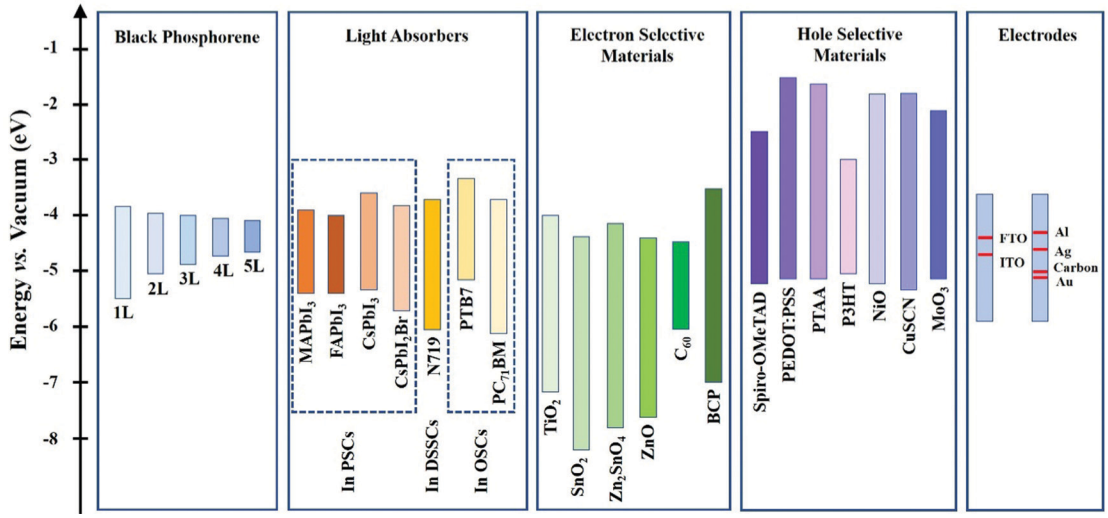

Fig. 3 Energy level diagram of black phosphorene (BP) and some representative materials commonly used in photovoltaics. The conduction band and valence band values of 1–5-layer BP are taken from ref. 27, which was determined from HSE06 calculation. PTB7: Poly[4,8-bis[(2-ethylhexyl)oxy]benzo[1,2-*b*:4,5-*b*′]dithiophene-2,6-diyl][3-fluoro-2-[(2-ethylhexyl)carbonyl]thieno[3,4-*b*]-thiophenediyl]; $PC_{71}BM$: phenyl-C71-butyric acid methyl ester; C60: buckminsterfullerene; BCP: bathocuproine; spiro-OMeTAD: 2,2′,7,7′-tetrakis-(*N*,*N*-di-4-methoxyphenylamino)-9,9′-spirobifluorene; PEDOT:PSS: poly(3,4-ethylenedioxythiophene):polystyrene sulfonate; PTAA: polytriarylamine; P3HT: poly(3-hexylthiophene).

the hole mobility in monolayer BP has been calculated to be 700 $cm^2\ V^{-1}\ s^{-1}$ in the *x*-axis and 26 000 $cm^2\ V^{-1}\ s^{-1}$ in the *y*-axis.[6,30] This extraordinarily large value of hole mobility for monolayer BP in the *y* direction is a consequence of the extremely small deformation potential (0.15 ± 0.03 eV) and occurs despite the fact that the carriers are very heavy ($6.35m_0$).[30] The carrier mobility of BP can be further modified with applied strain *via* tuning the effective masses.[31] Because BP has superior charge carrier mobilities to that of the majority of other semiconductors, it is particularly advantageous for the separation and transport of electrons and holes for optoelectronic applications.

2.4. Optical absorption

Because the bandgap of BP can be tuned from 0.3 eV in the bulk form to about 2.0 eV in the monolayer, the absorption spectrum of BP can cover a large range from infrared light to visible, which makes it a good candidate for various optical applications including solar cells. Optical absorption is intrinsically an electron–photon interaction, which normally occurs at band edges. Because BP has a layer number-dependent bandgap, the corresponding photo absorption spectrum also changes with the thickness of BP flakes. The optical bandgap of BP has been widely studied through both experimental measurements and theoretical calculations.[6,22,32–34] It has been reported that the absorption peak position for an N-layer BP can be expressed by the formula $E_{N,n} = 1.8 - 1.46\cos\left(\frac{n\pi}{N+1}\right)$, where *n* is the subband index, $n = 1 \ldots N$.[22] The direct optical absorption measurements demonstrated the optical band gaps of 1.38, 1.23, 1.05, 0.85, and 0.72 eV for 1–5 layers BP, respectively.[32] The optical properties of BP are also very anisotropic, with optical absorption being significantly dependent on the prototype orientation of BP. For example, BP absorbs polarized light in the *x* direction but is transparent to polarized light along the *y* direction.[16,30] The absorption coefficient of BP in the *x* direction is 10 times larger than that in the *y* direction, while the photon diffusion coefficient along the *x* direction is nearly 16 times higher than that in the *y* direction.[33,35] Since strain, external electrical field, functionalization, and doping have a significant effect on the band gap of BP, they can also be used to tune the optical properties of BP. For instance, a 4% compressive strain is reported to shift the optical band gap of BP to the infrared region (energies between 1.1 and 1.7 eV), while a 4% tensile strain enables absorption over almost the entire visible range.[33,36] The unique optical properties of BP, particularly the ability to modulate its absorption wavelength from the ultraviolet to near-infrared region, make it a promising material in solar-energy-conversion processes, including photocatalysis, photochemistry, and photovoltaics.

2.5. Environmental stability

The three-fold configured phosphorus atoms possess a lone electron pair in the BP structure, which can provide active sites for bonding with oxygen atoms.[37] Because of this, the few-layer BP prepared by mechanical exfoliation has been observed to readily degrade under ambient conditions. During degradation, BP has been found to initially form P_xO_y on the surface, which then further reacts with H_2O and gradually transforms into phosphoric acid. The oxidation-facilitated degradation of BP stands in sharp contrast to the behavior of metals, for which thin surface oxide layers have been found to prevent further oxidation.[38] The oxidation rate of BP has been found to correlate to several external conditions such as oxygen concentration, ambient humidity, and light exposure.[39]

Thus, improving the environmental stability of BP is crucial before it can be used in any future photochemical applications. Fortunately, many strategies including van der Waals interactive encapsulation between two h-BN layers, graphene contacts protection, and AlO_x layer passivation have been reported to preserve BP under ambient conditions for months.[40–43] In addition, the BP nanosheets produced by organic exfoliation showed improved water and light stability due to the encapsulation of BP surfaces by organic molecules.[32,44,45] BP nanosheets exfoliated in isopropanol were observed to be very stable without any noticeable aggregation at room temperature for two months in our previous work.[46] Notably, BP has been shown to be sufficiently stable for photovoltaic applications because its use as interfacial layers or additives keeps it from directly contacting the ambient atmosphere (Table 2).[46–48] This is not true for other applications in which BP is partly or entirely exposed to the ambient atmosphere (*e.g.*, field-effect transistors and catalysis).[49]

3. Scalable production of BP

Since BP was first synthesized *via* exfoliation in early 2014 using a scotch-tape microcleavage method,[2] various other techniques have been developed to synthesize ultrathin BP, which can be essentially divided into top-down and bottom-up methods. The facile, precise, scalable, and low-cost preparation of BP is the premise of its widespread application in photovoltaics. Therefore, an outline of BP preparation and synthetic routes that are likely to be adopted for large-scale implementation is provided in this section. In this context, some techniques for BP preparation which are only practical for use in laboratories for fundamental research currently, such as mechanical exfoliation,[2] plasma etching,[50] epitaxial growth,[51] *etc.*, are not discussed here. It is worth noting that two-dimensional layered materials can form other ultra-small nanostructures, including quantum dots (QDs). Though BP nanosheets will be the focus of this review, selective preparation of BPQDs is also included. Table 1 summarizes the key performance metrics of various techniques for BP preparation on a large scale. Currently, most BP preparation strategies utilize top-down methods as there are yet no quite promising bottom-up methods. More precise, controllable, and effective preparation of BP is still urgently needed for BP to meet its potential for use in optoelectronics.

3.1. Top-down approaches

3.1.1 Ultrasonic exfoliation. Ultrasonic exfoliation, which is usually performed through bath ultrasonication or probe

Table 1 Comparison of various techniques for scalable BP preparation

Technique		Precursor	BP nanosheets			Works for BPQD preparation?	BPQD uniformity	Key aspects
			Thickness	Lateral size	Sample uniformity			
Top-down approaches	Ultrasonic exfoliation	Bulk BP	Single to few layer	Tens of nanometers to micrometers	Low	Y	Low	Time-consuming
	Electrochemical exfoliation	Bulk BP	Single to few layer	Tens of micrometers	High	Y	Relatively high	Highly controllable, large lateral size
	Shear-assisted exfoliation	Bulk BP	Few layer	Hundreds of nanometers to micrometers	High	Y	High	Timesaving, high reproducibility
	Solvothermal exfoliation	Bulk BP	Few to multilayer	Several micrometers	Low	Y	Relatively high	Relatively time-consuming
	Microwave-assisted exfoliation	Bulk BP	Few to multilayer	Hundreds of nanometers to micrometers	Low	Y	Relatively high	Very timesaving, more suitable for BPQD preparation compared to nanosheets
	High energy ball milling	Bulk BP	Few layer	Tens of nanometers	Low	Y	Low	Relatively time-consuming, not suitable for BP nanosheets preparation
Bottom-up approaches	Pulsed laser deposition	Bulk BP	Single to few layer	Centimeter	High	—	—	Highly controllable; large lateral size, extreme reaction conditions
	Wet-chemistry synthesis	Red phosphorous; white phosphorus	Few layer	Tens to hundreds of nanometers	Low	—	—	Low crystallinity, easy oxidation

ultrasonication, is currently the most widely used top-down method for BP preparation. It offers a set of advantages, including a high yield, scalability, and solution processability. Solution processability is particularly important because it makes liquid phase exfoliation easily compatible with solution processes common in industrial processing, such as centrifugation and vacuum filtration. *N*-Methyl-2-pyrrolidone (NMP) was first selected as an exfoliation solvent to produce BP colloidal dispersions.[3] BP nanosheets with thicknesses ranging from 3.5 to 5 nm were obtained in NMP after 24 h of ultrasonication in a water bath. Since then, atomically thin BP nanosheets have been ultrasonically exfoliated in a wide range of organic solvents, including *N*-cyclohexyl-2-pyrrolidone (CHP),[52] dimethyl formamide (DMF),[32,53] dimethyl sulfoxide (DMSO),[32] isopropanol,[53,54] acetone,[53,55] and tetrahydrofuran (THF).[56] The yield of BP monotonically increases with the increasing boiling point and surface tension of organic solvent (Fig. 4a and b).[53] In addition to organic solvents, water[57,58] and ionic liquids[59] also enable stable and high-concentration dispersions of mono- to few-layer BP nanosheets through ultrasonication-assisted exfoliation. Additives such as NaOH[60] and phytic acid[61,62] have been introduced to further improve BP exfoliation *via* ultrasonication. Their abundant hydroxyl and phosphorus groups can intercalate into the BP interlayers and thus aid in exfoliation. Ice-assisted exfoliation carried out by pre-freezing bulk BP dispersion prior to ultrasonication is also developed to increase exfoliation efficiency and improve BP morphology.[63]

During ultrasonication, small voids are created by the ultrasound-generated alternating cycles of high and low pressure, which leads to the fragmentation of the BP nanosheets. Thus, extending sonication time facilitates the generation of BPQDs. However, preparing QDs *via* direct ultrasonic exfoliation usually results in a wide size distribution and relatively low yield. Thus, grinding and sonicating are usually integrated to boost the yield of high-quality BPQDs.[64–66] The integration of first probe and then bath sonication further enables the use of bulk BP crystals as raw materials in BPQD production, which also enhances the reproducibility of BPQDs compared to the grinding and sonicating methods.[67]

3.1.2 Electrochemical exfoliation. Electrochemical exfoliation is another facile, scalable, and economic strategy for 2D material preparation in which ions are driven by an external bias to intercalate interlayers and weaken interlayer vdW adhesion. Electrochemical exfoliation of BP was first conducted with bulk BP serving as the anode in an acidic aqueous solution of H_2SO_4.[68] Yet, the exfoliated BP nanosheets were more prone to oxidation, which is also favored by the anodic exfoliation process itself. In this context, cathodic exfoliation of BP was developed, and it was found to result in less BP oxidation than anodic exfoliation.[69–73] Different intercalating agents, such as tetrabutylammonium hexafluorophosphate,[69,72,74] tetra alkylammonium (TAA) tetrafluoroborate salts,[70,73] hexadecyltrimethyl–ammonium chloride,[71] and phytic acid[75] have been adopted for cathodic exfoliation of BP in an organic solvent or aqueous solution. In addition to nanosheets, BPQDs with a small lateral size of 6–8 nm are also prepared by judiciously engineering electrochemical exfoliation factors, such as applied potential, electrolyte composition, and especially the intercalating ions.[76,77] Recently, electrochemical anodic exfoliation has been readopted, and it interestingly demonstrates the exfoliation of BP nanosheets, BPQDs and zigzag-BP nanobelts *via* an oxygen-driven mechanism in an aqueous solution by simply changing the applied current densities to adjust the oxidation rate.[78]

3.1.3 Shear-assisted exfoliation. The main drawback of the ultrasonic exfoliation method is its time-consuming nature (taking at least several hours), which also negatively affects the lateral size of BP flakes both in terms of size and size homogeneity. In this context, shear-assisted exfoliation as an

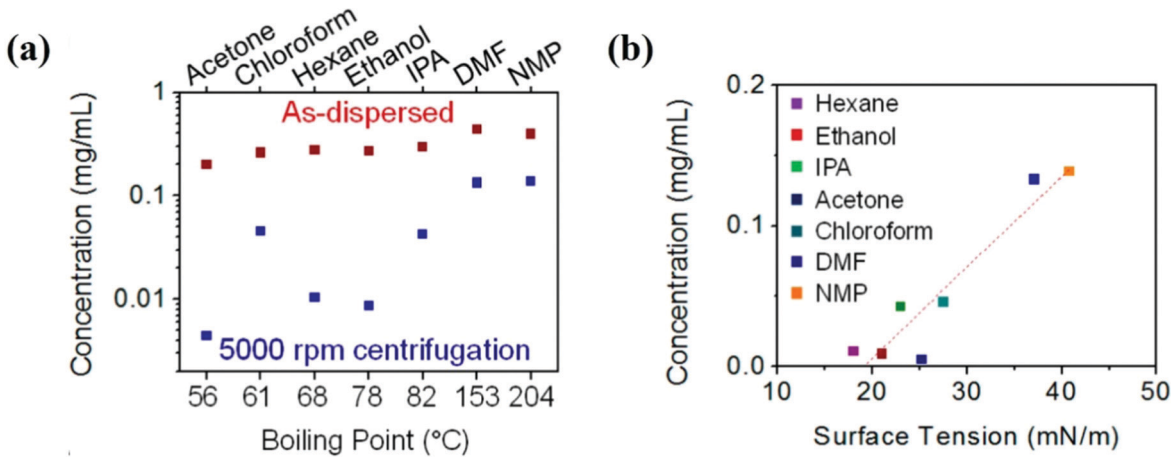

Fig. 4 Ultrasonic exfoliated BP concentration in various solvents (a) with different boiling points before and after centrifugation, and (b) with different surface tensions after centrifugation. Reproduced with permission from ref. 53. Copyright 2015, American Chemical Society.

alternative liquid phase exfoliation method to ultrasonic exfoliation is adopted to enable high yield BP production within a shorter time. A household kitchen blender, shear mixer and vortex fluidic device have been used to provide shear stress to break down interlayer van der Waals forces of the bulk BP crystals.[79–81] Highly crystalline mono- or few-layer-thick BP sheets on a micrometer scale can be obtained within only 30 min using shear exfoliation due to ultra-high turbulent shear rate. Particularly, a very narrow thickness distribution of BP nanosheets was observed *via* shear-assisted exfoliation compared to other liquid phase exfoliation methods.[80] BP nanosheets with a very narrow thickness distribution of 4.3 ± 0.4 nm were exfoliated using a vortex fluidic device.[80] In addition to the nanosheet counterpart, BPQDs with high yield were also produced using a household kitchen blender-assisted exfoliation.[82] The size of the produced BPQDs can reach up to ~2 nm with a thickness of only 0.58 nm (~1 layer).[82] These encouraging results demonstrate the promise of using shearing processes in scalable BP nanosheets and BPQD production.

3.1.4 Solvothermal exfoliation. Relatively high temperature and pressure promote the intercalation of solvent molecules into the interlayers of 2D materials, thus facilitating their exfoliation into nanosheets or QDs. In this context, solvothermal exfoliation was developed for BP preparation with a nitrogen-protected atmosphere applied to avoid the degradation of BP.[83–86] BP nanosheets have been prepared using solvothermal treatment followed by subsequent ultrasonic treatment.[83] The thickness and lateral size of BP nanosheets can be easily controlled by the ultrasonication time after solvothermal treatment. High-quality BP nanosheets with an average thickness of approximately 2 nm and a lateral size of up to 10 μm were obtained with only 1 h of ultrasonication after solvothermal treatment at 200 °C for 24 h.[83] With well-ground BP powders as the starting material, ultrasmall BPQDs can be prepared in large scale by using a solvothermal method even without further ultrasonic treatment. BPQDs within a range of 1–3 nm were prepared at a temperature of only 140 °C for 6 h *via* solvothermal exfoliation.[84–86]

3.1.5 Microwave-assisted exfoliation. Microwave-assisted exfoliation greatly shortens the time in fabricating high-quality BP on a large scale through the combined microwave and thermal effects.[87–90] Notably, few-layer BP nanosheets can be obtained in only several minutes with this approach.[87,88] Yet, the thickness and size homogeneity of the as-prepared BP nanosheets *via* microwave-assisted exfoliation are worse than those obtained with ultrasonic exfoliation. BP nanosheets consisting of few layers to multilayers (~18 layers) and lateral dimensions ranging from hundreds of nanometers up to ~4 μm were attained.[87] Although microwaves benefit the isolation of BP sheets, the increased temperature was found to facilitate the fragment of BP into small-sized QDs. It has been demonstrated that BP nanosheets can be produced at 50 °C for 10 min and BPQDs can be achieved at 120 °C for 30 min *via* microwave-assisted exfoliation.[90] Encouragingly, differing from its nanosheet counterpart, BPQDs prepared *via* microwave-assisted exfoliation possess both narrow thickness and size distributions (~2–4 nm).[90]

3.1.6 High-energy ball milling. Large shear forces generated from collisions during ball milling are widely used to exfoliate 2D materials. It is worth noting that the introduction of LiOH additives during ball milling facilitates BP nanosheet exfoliation and concurrently results in the functionalization of BP with increased stability.[91] Yet, similar to microwave-assisted exfoliation, ball milling tends to generate BP nanosheets with a broad thickness distribution (~0.7–6 nm, corresponding to ~1–8 BP layers).[91] Thus, ball milling is more frequently used for BPQD production.[92–94] The average diameter of BPQDs varies based on the milling period, speed, and solvent.[92] Ultra-small BPQDs were prepared *via* the liquid-based high-energy ball milling of bulk BP for 6 hrs with ethanol as the solvent.[93] The obtained BPQDs possess an average lateral size of 6.5 ± 3 nm and a thickness of 3.4 ± 2.6 nm. They are dispersed stably in ethylene glycol and stable for more than two weeks.[93] In addition to using bulk BP, BPQDs can also be fabricated directly *via* high energy mechanical milling of red phosphorous powder through 72 h of processing.[94]

3.2. Bottom-up strategies

Bottom-up synthesis represents an alternative approach to producing more precise 2D materials. Vapor deposition and wet-chemical synthesis represent the most widely used bottom-up routes for 2D material preparation. However, significant challenges exist for their application in BP synthesis due to lack of suitable precursors, the requirement of extreme reaction conditions, and stability issues.[95] Although large-scale BP nanosheets have been prepared *via* pulsed laser deposition[96] and wet-chemistry synthesis,[97] significant efforts are still needed to mitigate the rigorous reaction conditions and to increase the crystallinity of the as-prepared BP nanosheets in the future.

3.2.1 Pulsed laser deposition. The vapor deposition can be divided into chemical vapor deposition (CVD) and physical vapor deposition (PVD). Since most phosphorus precursors are highly toxic and not suitable for direct CVD, currently, BP nanosheets being made *via* CVD is carried out *via* the conversion between phosphorous allotropes.[98–103] Yet, the rigorous phase transition conditions, including high pressure, high temperature, and laser assisting, to yield high-quality crystalline BP, limit their wide applications for large-scale BP synthesis. In this context, PVD was developed as a more promising bottom-up technique for large-scale BP nanosheet production. Pulsed laser deposition is a PVD technique that was first developed to fabricate ultrathin (2–8 nm) BP films by using bulk BP as a target.[104,105] Amorphous BP thin films can be deposited at a moderate temperature of 150 °C under a vacuum of 1.5×10^{-7} Torr. Recently, an ultrahigh vacuum of $\sim 1.6 \times 10^{-9}$ Torr and a relatively increased temperature of 300 °C were adopted during pulsed laser deposition to enable the large-scale growth of crystalline BP nanosheets (Fig. 5a).[96] It was found that the plasma-activated region induced by laser ablation could provide highly desirable conditions for BP cluster formation and transport. Centimeter scale BP with precisely controlled thickness and high crystallinity were deposited on mica substrates *via* manipulating the number of laser pulses during deposition (Fig. 5b–e). Encouragingly, field-effect transistors based on the as-prepared large-scale BP films exhibited extremely high hole mobility of 213 and 617 $cm^2 V^{-1} s^{-1}$ at 295 and 250 K, respectively.[96] The encouraging results signify that pulsed laser deposition is a promising bottom-up method for scalable BP nanosheet synthesis in the future.

3.2.2 Wet-chemistry synthesis. Wet-chemistry synthesis is another bottom-up strategy for scalable BP production. Similar to vapor deposition of BP nanosheets, allotropes of BP are usually adopted as raw materials in solvothermal synthesis due to the toxicity of phosphorus precursors.[97,106,107] Polycrystalline BP nanosheets were first hydrothermally synthesized *via* the transformation of red phosphorous (RP) microspheres with ammonium fluoride (NH_4F) added to reduce the activation energy of RP and smoothen the surface of BP nanosheets.[106] White phosphorus (WP) has also been utilized as a raw material for the synthesis of BP nanosheets *via* a direct solvothermal process in an ethylenediamine system.[97,107] Gram-scale quantities of few-layer BP nanosheets (2–3 layers) can be produced *via* this approach with temperatures ranging from 60 to 140 °C.[97] Notably, the degradation of BP under oxidizing conditions remains a major challenge of using the

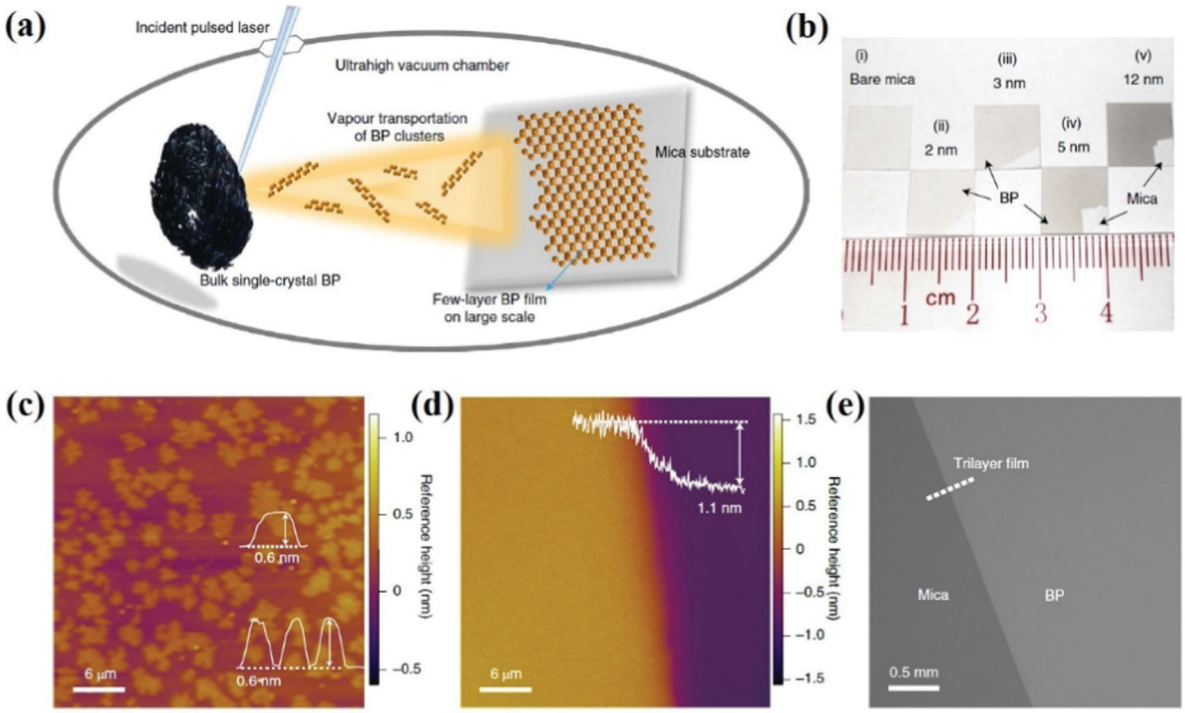

Fig. 5 (a) Schematic of the pulsed laser deposition process for BP fabrication; (b) photographs of the as-deposited BP films with different thickness; AFM images of (c) monolayer BP and (d) bilayer BP sheets; (e) electron back-scatter diffraction image of a trilayer BP. Reproduced with permission from ref. 96. Copyright 2021, Springer Nature.

hydrothermal method, but it can be mitigated by using boiling water to create an oxygen-free environment.

4. Strategies and working mechanisms of BP-incorporated solar cells

The development of liquid phase exfoliation, especially ultrasonic exfoliation, has significantly promoted the exploration of BP in various solar cells in the last five years. Until now, BP has been incorporated into a variety of solar cells, including OSCs, DSSCs, HJSCs, and PSCs. A detailed summary of the previous experimental studies on BP derivatives in PV devices is depicted in Table 2. Here, we focus on providing a concise overview and timely update on the successful experimental demonstration of BP in emerging solar cells. The function of BP and its effect on device performance are fully discussed.

4.1. BP-enhanced hole extraction and transport

BP is regarded as an intriguing candidate for next-generation carrier transporting materials because of its extremely high mobility for both electrons and holes. Investigation into the electric properties of polycrystalline BP reveals that it possesses good p-type conductivity and a positive Hall coefficient for undoped BP.[28] Due to its hole biased conductivity, BP was first utilized as a hole transporting material (HTM) in solar cells. The exploration of BP as a hole selective material was initially examined in 2016 *via* an OSC with a device structure of glass/ITO/PEDOT:PSS/BP/PTB7:$PC_{71}BM$/Ca/Al.[108] The BP-containing device was observed to possess decreased device performance (6.52%) compared to the control device without BP incorporation (7.72%). This decreased performance was attributed to the mismatched band structure of the BP layer with PEDOT:PSS and the electron donor material (*e.g.*, PTB7). The thermodynamically unfavorable hole transfer blocked hole transport near the anode, leading to a decrease in short circuit current (J_{sc}) and *PCE*. On the other hand, ambipolar BP might also encourage electron transport to the anode, which can trap holes and further lower the device performance.[108] This early work indicates the significance of precisely controlling BP thickness in applications due to its thickness-dependent bandgaps, which is distinct from other 2D counterparts. Though this initial study highlighted the

Table 2 Summary of research on the application of BP derivatives in various solar cells, where LPE refers to liquid phase exfoliation

Cell type	BP morphology	BP synthesis method	Device structure	Major BP function	PCE (%)	Ref.
OSC	Nanosheets	LPE (Bath sonication)	ITO/PEDOT:PSS/BP/PTB7:$PC_{71}BM$/Ca/Al	Hole extraction and transport	6.52	108
			ITO/ZnO/BP/PTB7:$PC_{71}BM$/MoO_3/Al	Electron extraction and transport	8.18	
OSC	QDs	LPE (probe sonication)	ITO/PEDOT:PSS/PTB7:$PC_{71}BM$ with BPQDs/Ca/Al	Light harvesting	8.60	109
			ITO/PEDOT:PSS/PBDTTT-EFT:$PC_{71}BM$ with BPQDs/Ca/Al		9.95	
OSC	—	Stirred overnight and filtration	ITO/PEDOT:PSS/PTB7-Th:$PC_{71}BM$:BP/PFN/Al	Hole extraction and transport	10.50	110
			ITO/ZnO/J71: ITIC:BP/MoO_3/Al		9.41	
			ITO/PEDOT:PSS/J71: $PC_{71}BM$:BP/PFN/Al		3.97	
OSC	Nanosheets	LPE (bath sonication)	ITO/ZnO/PTB7-Th:IEICO-4F with BP/MoO_3/Ag	Morphology modifier of photoabsorber	12.20	111
			ITO/ZnO/PBDB-T:ITIC with BP/MoO_3/Ag		9.70	
DSSC	QDs	LPE (probe and bath sonication)	FTO/PANI-BPQDs/electrolyte/dye/TiO_2/FTO	Light harvesting	6.85	112
DSSC	Nanosheets	LPE (bath sonication)	FTO/TiO_2-BP/dye/electrolyte/Pt	Electron extraction and transport	3.28	113
DSSC	QDs	Sonochemical method	FTO/TiO_2/N-719/BP-RPQD/electrolyte/Pt	Light harvesting	8.02	114
			FTO/TiO_2/BP-RPQD/electrolyte/Pt		0.12	
DSSC	Nanosheets	LPE (probe sonication)	FTO/TiO_2-BP/N719/electrolyte/Pt	Electron extraction and transport	9.73	115
HJSC	Dots	LPE (sonication)	ITO/ZnO/BP–PCBM/PEDOT:PSS/Ag	Donor in heterojunction	8.30	116
HJSC	QDs	Ball milling and LPE (bath sonication)	Al/ZnO:BP/Si/PEDOT:PSS/Ag	Electron extraction and transport	15.20	117
HJSC	Nanosheets	LPE (microwave-assisted)	Steel plate/GaIn/Si/BP–SWCNT/Cr/Au	Hole extraction and transport	9.37	118
HJSC	QDs	LPE (bath sonication)	Al/n-Si/PEDOT:PSS/BPQDs/Ag	Hole extraction and transport	13.60	119
PSC	Nanosheets	LPE (probe sonication)	FTO/TiO_2/$MAPbI_3$/BP/Spiro-OMeTAD/Au	Hole extraction and transport	16.40	120
			FTO/TiO_2/$MAPbI_3$/BP/Au		7.88	
PSC	QDs	LPE (bath sonication)	ITO/PEDOT:PSS/BPQD/$MAPbI_3$/PCBM/Ag	Hole extraction and transport	16.69	65
PSC	QDs	LPE (bath sonication)	ITO/BPQDs/$FA_{0.85}MA_{0.15}PbBr_{0.5}I_{2.5}$/Spiro-OMeTAD/Au	Electron extraction and transport	11.26	121
PSC	Nanosheets	LPE (bath sonication)	FTO/c-TiO_2/$CsPbI_3$/BP/CuSCN/Au	Exciton dissociation	14.17	122
PSC	QDs	LPE (bath sonication)	ITO/PTAA/$MAPbI_3$-BPQDs/PCBM/BCP/Ag	Morphology modifier of photoabsorber	20.00	48
PSC	Nanosheets	LPE (shear-assisted)	FTO/TiO_2:BP/Perovskite/Spiro-OMeTAD/Ag	Electron extraction and transport	17.85	80
PSC	Nanosheets	LPE (sonication)	FTO/TiO_2/SnO_2/$MAPbI_3$:BP/Spiro-OMeTAD/Ag	Morphology modifier of photoabsorber	20.23	123
PSC	QDs	LPE (bath sonication)	ITO/NiO_x/$CsPbI_2Br$/BPQDs/PCBM/$Zr(acac)_2$/Ag	Electron extraction and transport	12.20	124
PSC	Nanosheets	LPE (bath sonication)	ITO/TiO_2/BP-3/$Cs_{0.05}FA_{0.79}MA_{0.16}PbBr_{0.5}I_{2.5}$/BP-1/Spiro-OMeTAD/Ag	Electron and hole extraction and transport	19.83	46
PSC	Nanosheets	—	ITO/PTAA:BP/$MAPbI_3$/PCBM/BCP/Ag	Hole extraction and transport	20.49	47
PSC	QDs	LPE (probe and bath sonication)	ITO/SnO_2/$CsPbI_2Br$:BPQDs/Spiro-OMeTAD/Au	Morphology modifier of photoabsorber	15.47	125

challenges of using BP in PV applications, the feasibility and benefits of using BP with aligned bandgaps as HTM were quickly demonstrated by later studies on various photovoltaics, including PSCs,[46,47,65,120] OSCs,[110] and HJSCs.[118,119]

4.1.1 BP-enhanced hole extraction and transport in PSCs. Rapid advances in terms of PCE have been made in organic–inorganic hybrid PSCs with a certified champion power conversion efficiency of 25.5%, but this efficiency is still short of the theoretical Shockley–Queisser (S–Q) limit (~33%).[9] The poor electronic properties of carrier transport materials is one of the major challenges that hinders the progress of PSCs from achieving the S–Q limit. The most widely used HTLs (spiro-OMeTAD and PEDOT:PSS) possess hole mobilities less than $\sim 10^{-3}$ cm^2 V^{-1} s^{-1}, which is significantly lower than that of perovskite absorbers (*e.g.*, 10 cm^2 V^{-1} s^{-1} for $MAPbI_3$).[126,127] Because of their superior electronic and optoelectronic properties, BP QDs[65] and nanosheets[46,47,120] have been applied in PSCs to enhance hole extraction and transport by positioning them either at the HTL/perovskite interface[46,65,120] or by mixing with the original hole transport materials.[47]

The key to realizing BP-assisted hole transfer is to construct a cascade band energy alignment in the devices. BPQDs prepared by liquid exfoliation were first investigated as a hole extraction buffer layer on planar PSCs with an inverted p–i–n structure (Fig. 6a).[65] The well-matched band alignment of the BPQDs with both $MAPbI_3$ and PEDOT:PSS (Fig. 6b) boosted hole transfer from the perovskite to the PEDOT:PSS as confirmed by time-resolved photoluminescence (TRPL) spectroscopy (Fig. 6c). As a result, the devices with BPQDs inserted at the HTL/perovskite interface demonstrated a PCE of 16.69%, outperforming the control device fabricated without BPQDs (14.10%).[65] Particularly, BP nanosheets with suitable band energy have been investigated for use as the sole HTL in PSCs with a device structure of FTO/TiO_2/$MAPbI_3$/BP/Au.[120] Though the spin-coated BP nanosheet film was of poor quality and not optimized in thickness, a near doubling PCE (7.8%) compared to HTM free devices (4%) significantly verifies the powerful hole transfer ability of BP and suggests that it is a promising HTM for use in solar cells and optoelectronics devices.[120] Appealingly, the ambipolar nature of BP allows it to concurrently enhance carrier extraction at both the perovskite/HTL and ETL/perovskite interfaces *via* its bandgap tuning.[46] Cascade band energy alignments between BP nanosheet films, perovskite absorber, TiO_2 ETL, and spiro-OMeTAD HTL were concurrently attained by precisely tailoring the BP film thickness at the respective interface (yielding TiO_2 ETL/BP-3/perovskite and perovskite/BP-1/spiro-OMeTAD HTL) (Fig. 6d). The favorable band energy alignment facilitated cascade interfacial carrier extraction (Fig. 6e) and delivered an enhanced power conversion efficiency of 19.83% (with BP) compared to 16.95% (BP-free) (Fig. 6f).[46]

In addition to interface application, ultrathin BP nanosheets were also investigated as an additive to a poly(triarylamine) (PTAA) HTL to tune the work function and enhance hole transfer at the HTL/perovskite interface.[47] The Fermi level (E_F) of the BP:PTAA film was shifted 70 mV towards the highest occupied molecular orbital (HOMO) level, indicating the p-type doping of BP to PTAA. Accordingly, the work function of the hybrid HTL increased from 4.5 to 4.65 eV, decreasing the hole extraction barrier at the perovskite/HTL interface. In addition, coating a perovskite film on a BP:PTAA HTL was observed to enlarge the grain size and decrease the defects compared to that coated on PTAA. As a result, the corresponding device using the BP:PTAA HTL exhibited an improved PCE of 20.49% compared to the 18.26% of the control device.[47]

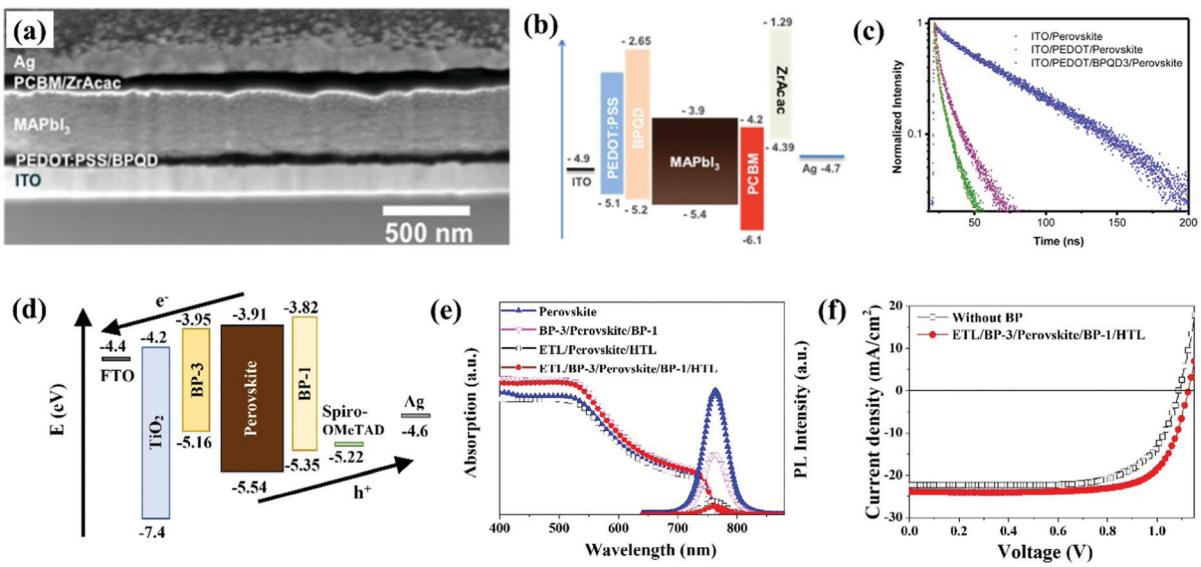

Fig. 6 (a) CS-SEM image and (b) energy level diagram in the PSC with BPQDs incorporated at the perovskite/PEDOT:PSS interface; (c) TRPL spectra of perovskite films with different interfaces. (a–c) Reproduced with permission from ref. 65. Copyright 2017, American Chemical Society. (d) Energy level diagram, (e) UV-vis and PL spectra, and (f) *J*–*V* curves of PSCs with dual-positioning of BP at both interfaces. (d–f) Reproduced with permission from ref. 46. Copyright 2020, John Wiley and Sons.

4.1.2 BP-enhanced hole extraction and transport in OSCs. OSCs, which are typically based on the blends of electron–donor materials that form bulk heterojunctions in devices, are considered as another potential alternative to silicon-based solar cells due to their low cost, light weight, mechanical flexibility, and the ability for large-area roll-to-roll coating processes.[128] Recent developments in materials science have led to a rapid increase in PCE for OSCs with values now reaching 17.4%.[9] One of the great challenges for improving the efficiency of OSCs lies in the relatively low carrier mobility of organic semiconductors which limits the charge collection efficiency in these devices. As a compromise, the thickness of the active layers in OSCs is usually limited to approximately 100 nm to ensure efficient charge transport.[110] However, this approach greatly restricts photo harvesting, and thus results in an unsatisfactory device performance.

Because of their inherently high charge carrier mobilities, BP nanosheets have been applied as a charge-transport mediator in OSCs *via* mixing with a PTB7-Th polymer donor and a PC71BM acceptor to construct a ternary blend film (Fig. 7a).[110] Particularly, the donor polymer PTB7-Th was found to facilitate the further exfoliation of BP nanosheets in a mixture of active materials due to the noncovalent interactions between PTB7-Th and BP. The incorporated BP nanosheets led to a 20% PCE enhancement (Fig. 7b) in a 150 nm thickened film due to increased J_{sc} resulting from enhanced charge transport and decreased carrier recombination.[110] The enhanced charge extraction was further attributed to improved hole extraction as determined by charge transport behavior studies on hole-only devices (Fig. 7c) and electron-only devices (Fig. 7d). This behavior was essentially due to the band energy level of the as-prepared BP nanosheets (inset in Fig. 7c and d).[110] Additionally, BP nanosheets were also found to increase the PCE when incorporated into OSCs with two different active layers (J71: $PC_{71}BM$ and J71: ITIC), which verified the generality of using BP to improve device performance through enhancing hole extraction and carrier transport.[110]

4.1.3 BP-enhanced hole extraction and transport in HJSCs. In addition to PSCs and OSCs, BP has also been incorporated into silicon (Si)-based HJSCs to improve device performance by enhancing the hole transport.[118,119] Hybrid Si-based HJSCs represent a high PCE cost-effective potential alternative to current crystalline Si solar cells. In hybrid Si-based HJSCs, a moderately doped n-type Si (n-Si) serves as the main absorber of solar photon flux and as the electron transport material. In this architecture, the adoption of an effective hole transporting phase is of key importance as it greatly influences the photovoltaic performance of the devices.

Organic/Si hybrid HJSCs, such as PEDOT:PSS/Si, are some of the most widely studied Si-based HJSCs due to their cost-effectiveness and facile fabrication. Similar to that in PSCs, solution-processed BPQDs were deposited at the PEDOT:PSS/Ag electrode interface in PEDOT:PSS/Si heterojunction-based solar cells for improved hole transport and collection.[119] A detailed UPS analysis indicated a 0.25 eV shift in work function at the PEDOT:PSS/BPQDs interface compared to PEDOT:PSS, which eliminated the potential barrier between the Ag electrode and PEDOT:PSS and thus led to more efficient hole transfer from PEDOT:PSS to the Ag electrode.[119] Carbon nanotube (CNT)/Si heterojunction-based solar cells are another cheaper potential

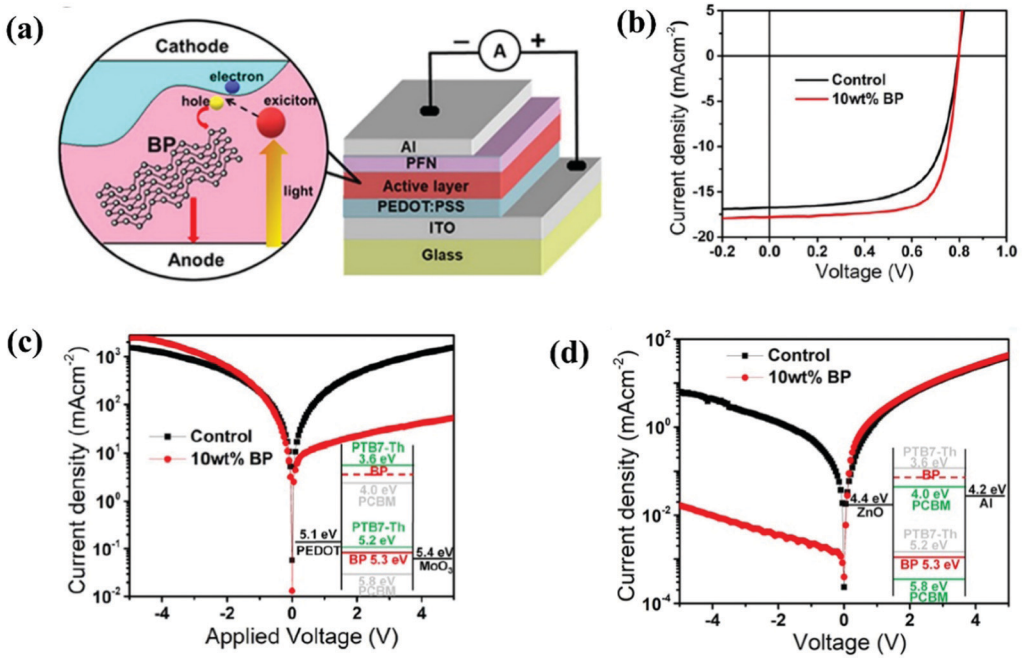

Fig. 7 (a) Device architecture of the OSC and schematic illustration of BP-assisted hole transfer in the active layer; (b) *J*–*V* curves of the OSCs w/wo BP incorporation under the illumination of AM 1.5G; *J*–*V* curves obtained for (c) hole-only and (d) electron-only devices based on control PTB7-Th:$PC_{71}BM$ blend film w/wo BP loading, inset shows the energy diagrams of devices. Reproduced with permission from ref. 110. Copyright 2018, Elsevier.

alternative to the current crystalline Si solar cells. Since the first report of CNT-Si solar cells, this field has seen rapid advances with PCEs reaching ~17%, but performance still lags behind that of crystalline Si solar cells.[129] The reduced PCE of CNT/Si HJSCs has been attributed to two aspects: the sparse network (nanotube junction) and poor hole selectivity of CNTs (due to its relatively low work function (~4.8 eV)).[130] In this context, ultrathin 2D nanostructured BP nanosheets with extremely high p-type conduction were introduced into a single-walled CNTs (SWCNTs)/Si heterojunction interface by physically mixing with SWCNTs.[118] The incorporation of BP resulted in a denser and more continuous network, which led to the reduced transparency of the BP-SWCNT film compared to the SWCNT film. However, the solar cells fabricated with the hybrid BP-SWCNT/Si heterojunctions still showed higher PCEs, indicating that the BP flakes exert a positive influence on the electronic states of the heterojunction. DFT calculations further revealed a donor–acceptor relationship between BP and CNTs, where BP was the donor and CNT was the acceptor. The transfer of electrons from BP to the CNTs slightly n-doped the nanotubes, which widened the depletion region on the CNT side of the CNT/Si heterojunction interface. This in turn improved the hole transfer from Si to the BP-SWCNT film and reduced charge recombination at the interface.[118]

4.2. BP-enhanced electron extraction and transport

BP can be applied as either an anode or a cathode due to its ambipolar conduction, readily tunable thickness-dependent bandgap, and favorable work function and Fermi level. Thus, in addition to utilizing BP in the anode for hole extraction and transport as discussed in Section 4.1, BP has also been investigated as a cathode material for electron extraction and transport in solar cells. Already, BP has been used to facilitate electron transfer in OSCs,[108] PSCs,[46,80,121,124] DSSCs[113,115] and HJSCs.[117] BP can be incorporated into the devices in multiple ways, including as a buffer layer between the ETL and photoactive layer,[46,108,124] mixed within the existing ETL,[80,113,115] and even as the sole ETL.[121] Same as the BP-enhanced hole extraction and transport, the cascade band energy alignment in the devices is the key to BP-enhanced electron extraction and transport.

4.2.1 BP-enhanced electron extraction and transport in OSCs. As discussed in Section 4.1.2, the organic semiconductor-based active layers in OSCs exhibit relatively low carrier mobility which significantly limits their charge collection efficiency and photovoltaic performance. In this context, solution exfoliated BP nanosheets were incorporated at the interface to enhance charge extraction.[108] Specifically, BP nanosheets were explored as both an HTM and ETM *via* interface insertion in OSCs with conventional and inverted structures (Fig. 8a). However, due to the mismatched band structure of the BP layer with PEDOT:PSS and the electron donor material (*e.g.*, PTB7), a decreased device performance was obtained (Fig. 8b). In contrast, enhanced photovoltaic performance from 7.37% to 8.18% (Fig. 8c) was observed when BP was coated on ZnO as an electron extraction layer due to the favorable band structure between the ZnO, BP, and $PC_{71}BM$ acceptor (Fig. 8d), which thermodynamically favored efficient electron transfer and prohibited carrier recombination near cathodes. The thickness of the BP layer at the ZnO/$PC_{71}BM$ interface was determined to be 10 nm.[108] This study highlights the significance of precise control

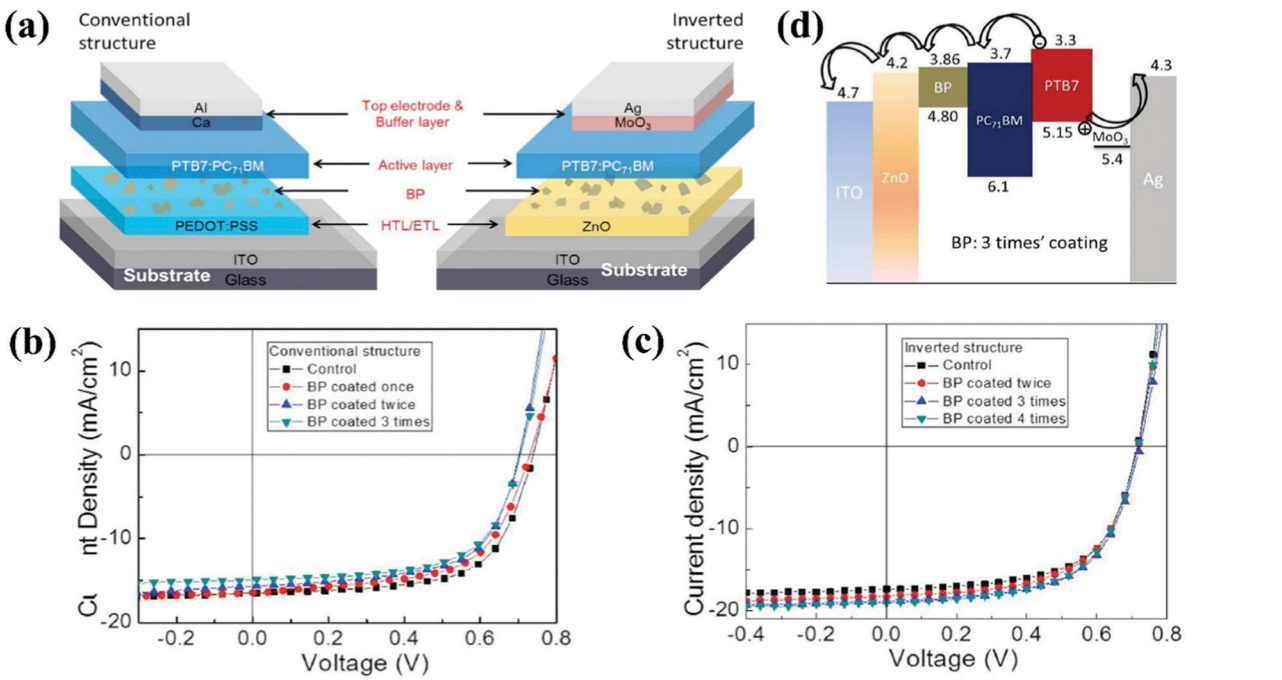

Fig. 8 (a) Conventional and inverted architectures of OSCs based on PTB7/$PC_{71}BM$; (b) *J*–*V* curves of OSCs with BP incorporated as an HTM; (c) *J*–*V* curves of OSCs with BP incorporated as an ETM; (d) energy band structure of the OSC with the incorporation of BP as an ETM. Reproduced with permission from ref. 108. Copyright 2016, John Wiley and Sons.

of the energy band structure of BP through thickness tailoring for practical applications.

4.2.2 BP-enhanced electron extraction and transport in PSCs. The ETL, which also functions as a hole blocking layer, represents a key component for high-efficiency PSCs. TiO_2 and SnO_2 are the two most widely used ETL materials in PSCs, but they still suffer from some electronic and stability shortfalls. The electron mobility of a TiO_2 ETL is less than 1 $cm^2 V^{-1} s^{-1}$, which is two orders of magnitude lower than that of the perovskite absorber.[131] The relatively lower conduction band edge of SnO_2 ETL results in severe charge recombination in the corresponding devices.[132] The ability to improve the charge transfer properties of existing ETMs and enhance the electron extraction at the ETL/perovskite interface represents an important endeavor towards high-efficiency PSCs. To this end, BP (with extremely high electron mobility) has been adopted in PSCs to enhance electron extraction and transport *via* either integrating within other ETMs (though interface modification[46,124] or mechanical mixing[80]) or working as the sole ETL.[121]

BPQDs were utilized as the sole ETL for flexible planar PSCs (Fig. 9b).[121] The average crystallite size of the BPQDs prepared by ultrasonication-assisted liquid phase exfoliation was determined to be $\sim 4.7 \pm 1.6$ nm, with an average thickness of 1.52 ± 0.5 nm (Fig. 9a) (corresponding to a stack of 3 ± 1 layer thick). Though a higher hole mobility was observed for BPQDs in this study, the energy band structure suggested that it is an electron transporting material for facilitating electron transfer but rejecting hole injection from the perovskite absorber to the BPQD-based ETL (Fig. 9c). The PSCs deposited on the BPQD-based ETL exhibited excellent electron extraction (Fig. 9e and f), resulting in a 3.15-fold PCE increase over that of the devices without an ETL (Fig. 9d).[121] In addition to building the ETL, BPQDs were also used to modify the perovskite/ETL interface in low-temperature (<180 °C) processed inorganic PSCs with a device structure of glass/ITO/NiOx/$CsPbI_2Br$/BPQDs/PCBM/$Zr(acac)_4$/Ag.[124] Interestingly, small BPQDs with an average size of 3.6 ± 0.5 nm were able to fill in the voids between the perovskite grains and thus optimize the morphology of the $CsPbI_2Br$ film. The embedded BPQDs were found to provide more pathways for electron extraction and thus effectively suppress charge recombination. As a result, the low temperature processed devices (<180 °C) exhibited a maximum PCE of 12.2%, which outperformed most of the previously reported $CsPbI_2Br$ based PSCs fabricated at higher temperatures.[124] Similar to BPQDs, BP nanosheets have also been incorporated into PSCs to improve electron extraction and transport.[46,80] Highly uniform thin BP nanosheets (4.3 ± 0.4 nm, five-layer thick) synthesized by shear-exfoliation were mixed with TiO_2 for efficient electron transport in a planar n–i–p PSC with a typical device structure of FTO/TiO_2:BP/Perovskite/Spiro-OMeTAD/Ag, leading to a PCE increase from 14.32% to 16.53%.[80] Likewise, placing 3- to 4-layer-thick BP nanosheets at the TiO_2 ETL/perovskite interface was also observed to enhance electron transfer due to the cascade electron transfer path together with the superior carrier mobility of BP.[46]

4.2.3 BP-enhanced electron extraction and transport in DSSCs. TiO_2 nanoparticle-based films are the most widely used photoanode in DSSCs, but they suffer from slow electron transport which results in a high rate of charge recombination between the TiO_2–dye and the TiO_2–electrolyte.[133] The development of photoanodes with efficient electron injection and fast charge transfer represents an important step towards

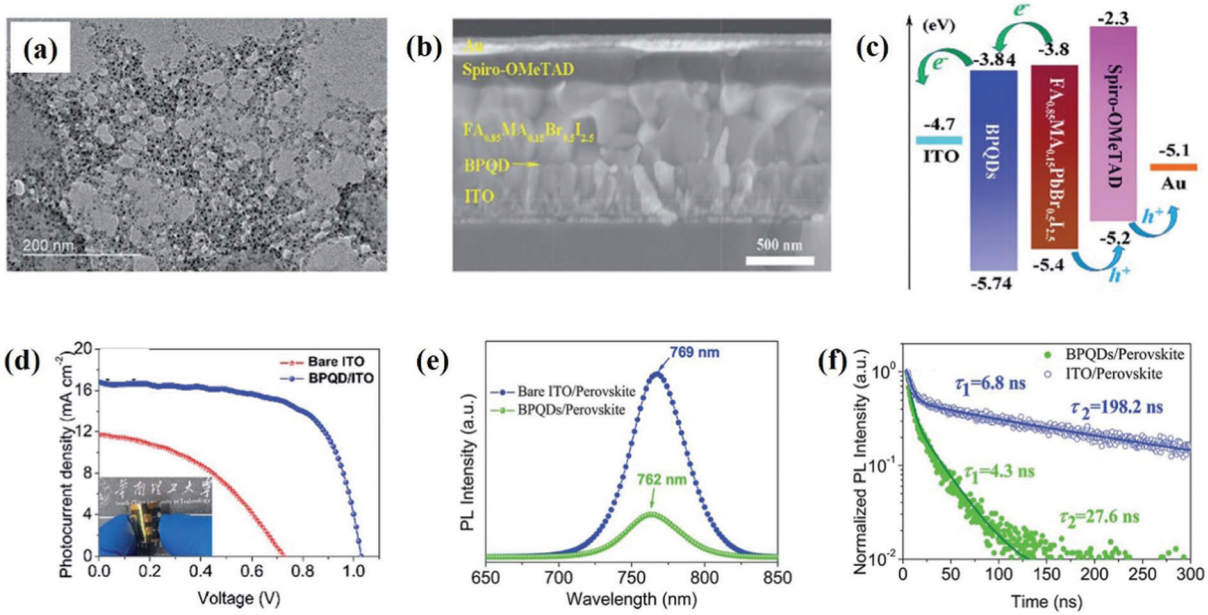

Fig. 9 (a) TEM image of the BPQDs; (b) CS-SEM image of and (c) energy level diagram in the PSCs; (d) *J*–*V* curves of PSCs w/wo BPQD ETL under 1 sun illumination (inset shows the digital image of the plastic PSC); (e) photoluminescence (PL) and (f) time-resolved PL (TRPL) decay trace of the perovskite film deposited on the ITO/PEN substrate w/wo BPQD ETL. Reproduced with permission from ref. 121. Copyright 2018, The Royal Society of Chemistry.

high-efficiency DSSCs. In this context, BP nanosheets with extraordinary electronic properties and charge carrier mobility have been adopted *via* mixing with TiO_2 as the composite photoanode in DSSCs.[113,115] In addition to forming a stepwise charge transfer path, the incorporation of the 2D BP nanosheets with large size could provide much shorter pathways for electron transfer compared to TiO_2 nanoparticles.[115] Furthermore, detailed characterization revealed an interfacial interaction between BP and TiO_2 *via* the formation of Ti–O–P bonds, which was further found to function as an efficient electron trap site and facilitate photogenerated electron–hole separation and inhibit charge recombination. Consequently, DSSCs with BP nanosheets acting as charge transport channels in TiO_2 photoanodes were found to enhance device performance from 6.98% to 9.73%.[115] For future studies, the replacement of TiO_2 nanoparticle-based photoanode with BPQDs and its further modification with BP nanosheets may provide better results and merit in-depth exploration for application in DSSCs.

4.2.4 BP-enhanced electron extraction and transport in HJSCs. In silicon (Si) based organic/inorganic HJSCs, the rear contacts for electron collection are usually made of metal layers (such as aluminum (Al), titanium/silver, or indium/gallium alloys) deposited on the back sides of Si wafers as dopant-free electrodes.[117] Unfortunately, the direct contact between the metal electrodes and Si substrates can lead to large Schottky barriers, which increase series resistances, weaken electron collection, and thus decrease the performance of the heterojunction devices. The ohmic contact between the metal and Si can be achieved *via* the ionic doping of the Si surface, but high temperatures of up to 800 °C, hazardous doping gases, and expensive facilities are needed during this doping process.[117,134] Thus, applying novel suitable materials as efficient interface electron-selective contacts is of great relevance.

Liquid-phase exfoliated BP nanoparticles integrated with ZnO were inserted between Si and the Al layer to facilitate electron transfer at the rear contact in a PEDOT:PSS/Si HJSC (Fig. 10a).[117] This doping allowed infrared light (>1100 nm) that penetrated through Si to be harvested by BP and generate photo-carriers, which were then found to transfer to ZnO (Fig. 10c). The charge injection from BP to ZnO significantly

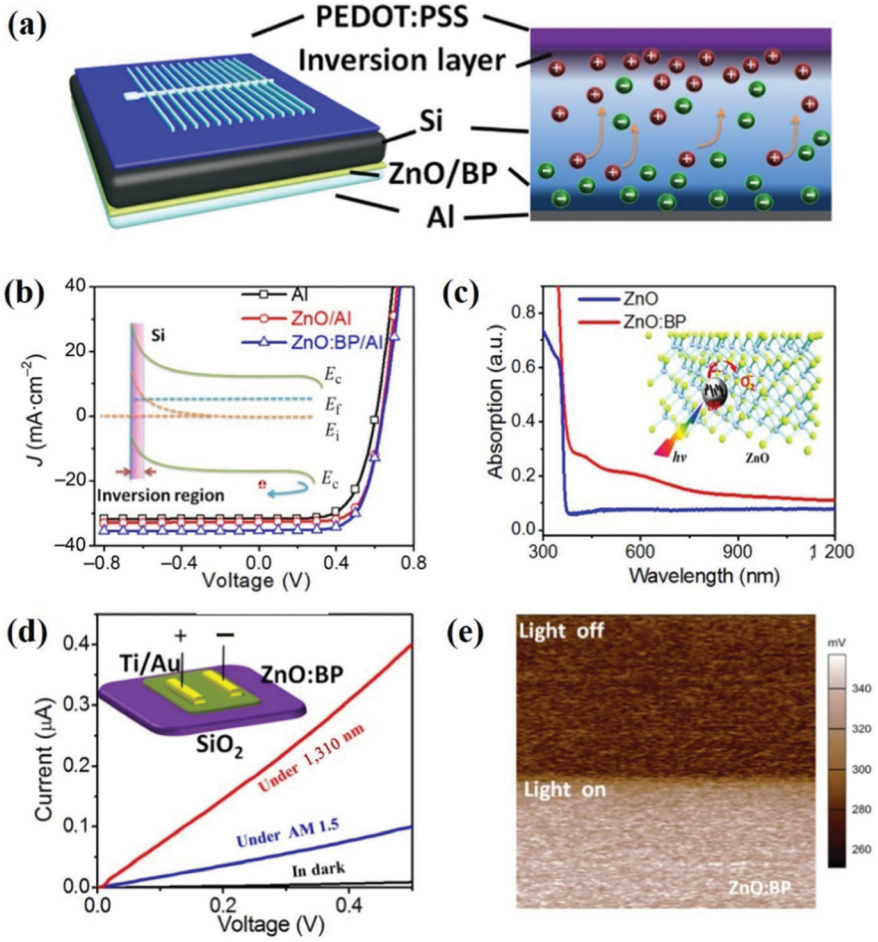

Fig. 10 (a) Schematic images of the device structure and carrier distribution induced by the electric field from the ZnO:BP interlayer; (b) *J*–*V* curves under solar-simulated AM 1.5; (c) UV-vis absorption spectra of ZnO and ZnO:BP films (inset shows BP nanoparticles under illumination may inject electrons into ZnO); (d) *I*–*V* curves of photodetector devices based on ZnO:BP; (e) surface potential images of ZnO:BP measured in the dark (top) and under 1310 nm illumination (bottom). Reproduced with permission from ref. 117. Copyright 2017, Springer Nature.

increased its conductivity (Fig. 10d) and lowered its work function (Fig. 10e), leading to a reduced energy barrier between Si and the Al electrode (inside Fig. 10b). In addition, the electron accumulation in ZnO:BP interlayers (resulting from BP absorption) produced a strong rear electrical field at the ZnO:BP/Si interface that prevented holes from reaching the back surface and suppressed charge recombination. Longer electron lifetime and diffusion length were detected upon the incorporation of the ZnO:BP layer. Consequently, the incorporation of the ZnO:BP layer enhanced the performance of the PEDOT:PSS/Si HJSC by 17%, resulting in a PCE of 15.2%.[117] The intriguing light-induced photo-doping enabled by BP not only demonstrated a novel approach for creating effective charge transport layers in optoelectronic devices, but it also enlightens its application in the photoactive layer for enhanced light absorption and harvesting, as discussed in detail in Section 4.3.

4.3. BP-enhanced light absorption

The broadband light absorption and high absorption coefficient of BP also make it a promising material for light harvesting in photoelectric devices.[16,67] The absorption spectrum of BP covers a large range from infrared to visible light depending inversely on the thickness of BP. Notably, BP exhibits a high absorption coefficient in a broad wavelength region, which is much higher than that of organic semiconductors with the same thickness.[16] It has been demonstrated that one- or two-layer BP films, which are less than 2 nm thick, can absorb approximately 10% of the light in the visible region.[135,136] Therefore, BP is considered to be an attractive additive in existing PV systems to enhance and expand light harvesting, or even act as the sole light absorber. Enhanced light harvesting *via* BP incorporation has already been demonstrated in OSCs[109] and DSSCs.[112,114] These studies either mixed BP into the light absorber or inserted BP as a supplementary absorption layer. Furthermore, improved light absorption has also frequently been reported in PSCs when BP is introduced for other purposes (*e.g.*, facilitating carrier extraction or assisting perovskite crystallization[46,47,124,125]).

4.3.1 BP-enhanced light absorption in OSCs. Due to the relatively low carrier mobility of organic semiconductors, the thickness of the organic photo-active layer in OSCs is usually limited to ~100 nm.[109,110] Consequently, the inadequate thickness of the active layer greatly restricts photo harvesting in OSCs compared to their inorganic counterparts. Adding photo absorption additives with high conductivity, such as plasmonic nanoparticles and conjugated polymers, has been demonstrated to be an effective approach to boost light harvesting and maintain efficient charge transfer.[137,138] In light of these two goals, BP stands out as an ideal photo additive in OSCs. Thus, solution-prepared BPQDs were incorporated into the active layers of two representative OPVs based on PTB7:$PC_{71}BM$ and PBDTTT-EFT:$PC_{71}BM$ to boost light harvesting.[109] The bandgap of the BPQDs was tuned by changing their size and thickness to form a cascade band structure (Fig. 11b). As expected, the construction of the efficient ternary OSC exhibited improved device performance mainly with an increased J_{sc} (Fig. 11c) resulting from better photo response. The enhanced light harvesting from BPQD incorporation was further attributed to two aspects. On one hand, BPQDs displayed strong absorption from UV to 750 nm (Fig. 11d), which improved light harvesting in the ternary active materials (Fig. 11e). On the other hand, since the diameter of the BPQDs (~4.5 nm) is much smaller than the wavelength of the incident light, Rayleigh scattering induced by BPQDs occurred in the devices, which in turn further enhanced light harvesting (Fig. 11f). Notably, a 10% improvement in PCE was obtained with only 0.055 wt% incorporation of BPQDs in this work, which is one to three orders of magnitude lower than the amount of any other additives previously applied in OSCs.[109]

4.3.2 BP-enhanced light absorption in DSSCs. Traditional DSSCs are generally composed of an active photoanode (*e.g.*, TiO_2) sensitized with a visible light-absorbing dye (such as N719) and a passive cathode. Although great progress in PCE has been achieved with this structure, it still suffers from poor infrared light absorption, which constitutes up to 49% of the solar spectrum. In this respect, expanding the light harvesting region to near-infrared represents an important endeavor towards high-efficiency DSSCs. Due to its broadband light absorption in the infrared region, BP is considered a promising bridge to enhance the absorption of DSSCs. Broadened light absorption to NIR *via* BP incorporation in DSSCs was realized by fabricating a BPQD-based photocathode for use in quasi-solid-state bifacial n-type DSSCs.[112] The BPQD-based photocathode was synthesized *via* positioning the as-prepared BPQDs into a polyaniline (PANI) matrix. Specifically, BP was observed to increase the device performance by both enhancing light harvesting and facilitating charge transfer.[112] In another study, a mixture of BPQDs and RPQDs (BP/RPQDs) has been integrated with the N719 dye to enhance light harvesting in DSSCs.[114] The BP/RPQDs were facilely synthesized with RP as the starting material *via* a sonochemistry-assisted method. Carriers generated from the long-wavelength light absorption of BP/RPQDs were found to inject into the LUMO of N719, and the corresponding increased photoelectron density at the photoanode further contributed to an increased J_{sc} and PCE.[114] Notably, BP/RPQDs were also explored as the only sensitizer in this work.[114] The sample DSSC composed of a BP/RPQD-sensitized mesoscopic TiO_2 photoanode, an I_3^-/I^- redox electrolyte, and a platinum electrode demonstrated a PCE of 0.12%. The low PCE was ascribed to charge carrier recombination at the BP/RPQDs/triiodide ions interface due to the large energy barrier and inferior charge injection from BP/RPQDs to TiO_2 due to the weak physical adsorption affinity between them.[114] Though the obtained PCE is much lower than state-of-the-art DSSCs, this pioneering work provides a foundation for using BP-based sensitizers to develop wide-spectra and high-efficiency DSSCs, and by extension, other solar cells with BP as a light harvesting material.

4.3.3 BP-enhanced light absorption in PSCs. Metal halide perovskites possess large absorption coefficients, high ambipolar carrier mobility, and long carrier diffusion length.[10] These outstanding optoelectronic properties enable the fabrication of thin film PSCs with desired light absorption. Because of this, BP

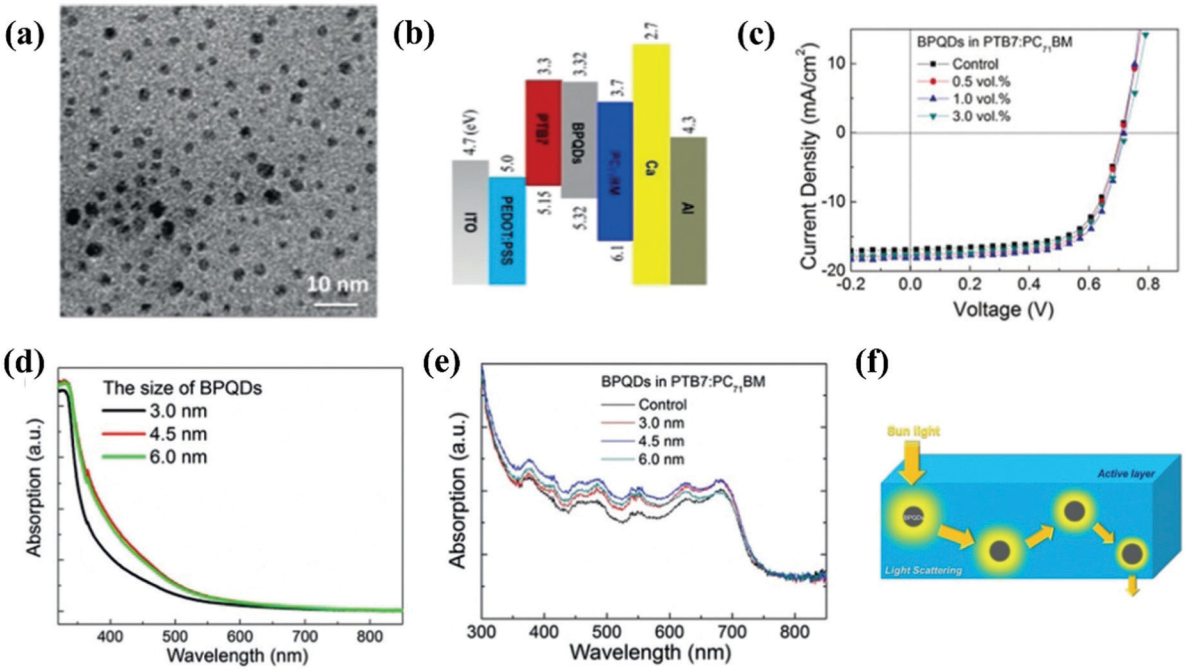

Fig. 11 (a) TEM image of BPQDs with an average diameter of 4.5 nm; (b) energy band structure and (c) *J*–*V* curves of the OSCs with the incorporation of BPQDs (size 4.5 nm) in the bulk heterojunction active layer; UV/vis absorption of (d) BPQDs and (e) PTB7:PC71BM layer with BPQDs in different sizes; (f) schematic diagram of light absorption and scattering by BPQDs in an organic layer. Reproduced with permission from ref. 109. Copyright 2017, John Wiley and Sons.

has not been investigated to improve light harvesting in PSCs. While not the primary goal, enhanced light absorption has frequently been reported when BP is incorporated in PSCs for other purposes such as carrier extraction and transport and assisting perovskite crystallization.[46,47,124,125] The mechanisms of BP-enhanced light absorption have been demonstrated to be highly dependent on its morphology and how it is integrated into PSCs. In most of the investigations with increased light harvesting *via* BP incorporation, improved perovskite crystallinity, large crystal grain size, and decreased defects have also been concurrently observed.[46,47,124,125] The enhanced light harvesting has thus been attributed to reduced light reflection and transmission resulting from the improved perovskite crystallinity and grain size.[47] In another representative study, improvement in light harvesting was observed when BP nanosheets with tailored thickness were concurrently inserted at both the ETL/perovskite and perovskite/HTL interfaces.[46] The improved harvesting was ascribed to the formation of a van der Waals heterostructure between the 2D BP nanosheets and perovskite absorber. It has been reported that charge redistribution occurs at the interface in van der Waals heterostructures which facilitates electron–hole pair separation and in turn leads to enhanced optical properties.[139]

Despite these studies discussed above, some reports claim that no significant difference in light harvesting is observed with BP incorporation in PSCs.[48,80,123] This could be due to insufficient amounts of BP additives or detection limits as perovskite absorber matrixes possess excellent absorption properties. These conflicting studies highlight that careful monitoring is needed for the study of BP in PSCs due to the multifunctional nature of BP.

4.4. BP-based heterojunction solar cells

The p–n heterojunction, which exhibits many intriguing optoelectronic properties, is the foundation in the design of some PV systems. Sandwiching p-type and n-type semiconductor materials (as donors and acceptors, respectively) results in the effective separation of charge carriers at the heterojunction interface and thus produces a flow of electricity. However, to be considered for photovoltaic applications, the heterojunction additionally needs a small direct bandgap of roughly 1.2–1.6 eV for efficient light absorption, and a high carrier mobility. In the shade of these two aspects, BP stands out as a promising candidate to construct HJSCs. BP-based HJSCs were first widely explored in theory by calculations.[140–146] 2D BP nanosheets have been investigated as donor materials with a variety of acceptor materials, such as GaN and 2D transition metal dichalcogenides (TMDCs, *i.e.*, MoS_2, ZrS_2, $MoTe_2$).[140–143] The heterobilayer or trilayer BP/TMDC-based 2D HJSCs with ultrathin thickness were predicted to enable a high theoretical maximum PCE of ~18%.[140,141] Particularly, 2D van der Waals heterojunctions could be constructed with a single type of material derived from BP *via* edge modification for use as donor and acceptor materials due to the ambipolar transport properties of BP.[145,146] PCE as high as 20% was demonstrated in the edge-modified BP-based HJSCs.[145]

The promising results from these theoretical studies have motivated experimentalists to explore BP-based HJSCs. In this

context, BP has been integrated with [6,6]-phenyl-C61-butyric acid methyl ester (PCBM) to form hybrid heterojunctions for solar cells.[116] PCBM is a well-known and widely used acceptor with efficient electron transport properties. Thus, BP was applied as an inorganic donor component and served as the hole transporting phase. Two distinct BP/PCBM heterojunctions (planar and bulk) were crafted through a crystallization/precipitation method (Fig. 12a). BP dots with an average size of $\sim 4.5 \pm 1.1$ nm were prepared with a height of $\sim 1.8 \pm 0.4$ nm (equivalent to ~ 3 layers) to match the energy level of PCBM for improved charge transport (Fig. 12b). The charge transfer between the donor BP and the PCBM acceptor resulted in a red-shifted broad absorption peak in the range of 400–600 nm (Fig. 12c), which is because neither BP nor PCBM displays notable absorption peaks in that range. The enhanced optical properties and superior carrier mobility of the BP/PCBM hybrid heterojunction led to favorable photovoltaic performances of 6.8% and 8.3% for planar and bulk heterojunctions, respectively.[116] This was the first example of BP-based heterojunctions for PV applications, and they demonstrated various advantages, such as the absence of heavy metals for reduced toxicity, good stability in liquid electrolytes, and tunable energy levels to match electrodes. The obtained promising result can be used as an important reference to promote further development of BP-based heterojunctions with high energy conversion efficiency.

4.5. BP-enhanced exciton dissociation

Solar cells can broadly be divided into two distinct classes according to their photophysical mechanisms for charge generation: (1) those that generate free electrons and holes and (2) those that generate bound electron–hole pairs (excitons). Notably, PSCs exhibit both free charges and excitons.[147] Recent studies have converged on the theory that free charge carriers are the dominant species in perovskites, yet the coupling of the excitons to the photons and their subsequent dissociation into free charge carriers are the central primary processes in device photophysics.[148] In organic–inorganic perovskites, such as the widely studied $CH_3NH_3PbI_3$, exciton binding energy can be as low as 2–20 meV, which is smaller than the intrinsic thermal energy at room temperature ($kT \approx 25$ meV),[149–151] and thus nearly full dissociation of excitons occurs in organic–inorganic halide perovskites. This suggests that the beneficial optoelectronic properties of organic–inorganic perovskites are due to the spontaneous free-carrier generation following light absorption. However, a much higher binding energy of around 86 meV has been reported for fully inorganic perovskites.[152] The larger energy barrier for exciton dissociation in inorganic perovskites

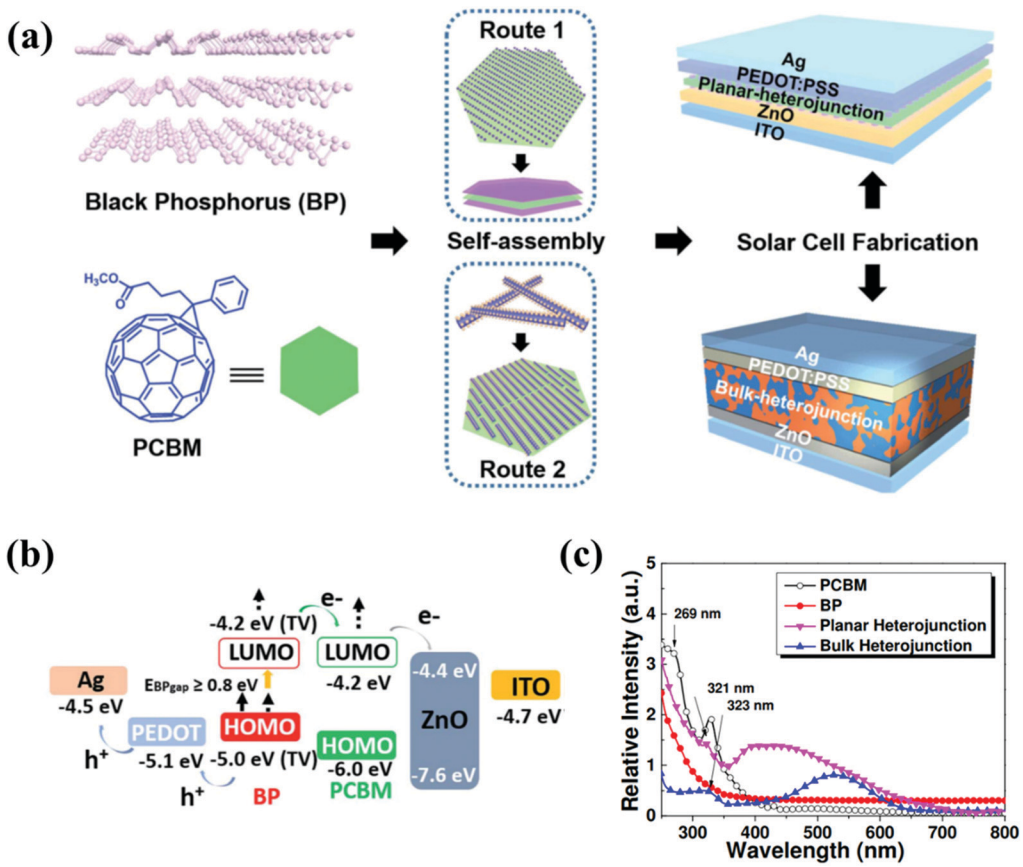

Fig. 12 (a) Schematic of BP/PCBM planar and bulk heterojunction-based solar cells; (b) energy level alignment in the device based on a BP/PCBM heterojunction (TV means theoretical value); (c) UV absorbance of BP, PCBM and BP/PCBM heterojunctions. Reproduced with permission from ref. 116. Copyright 2017, The Royal Society of Chemistry.

results in poor short-circuit current density in the corresponding devices and is regarded as one of the major challenges restricting PCE in inorganic PSCs.

Exciton binding energy is significantly affected by the built-in field across photovoltaic layers,[153,154] which provides an effective approach to tailor exciton binding energy. In this context, exciton dissociation in $CsPbI_3$-based PSCs with multilayer BP nanosheets positioning at the perovskite/HTL interface (Fig. 13a) was investigated.[122] BP insertion was found to increase the relative dielectric constant at the $CsPbI_3$/HTL interface (Fig. 13f) due to the BP's strong out-of-plane dielectric screening effect.[155] A higher relative permittivity corresponds to smaller Coulombic interactions between electrons and holes, which results in diminished exciton binding energy.[156] Thus, the exciton binding energy gradually decreased from 103.0 ± 8.2 meV of pure $CsPbI_3$ to 47.2 ± 9.0 meV of $CsPbI_3$–BP_{1-2} heterostructures (Fig. 13c).[122] The smallest exciton binding energy was obtained with BP_{1-2} due to its suitable bandgap structure in concurrently transferring holes and blocking electrons near the cathode (Fig. 13b). The decreased exciton binding energy after the insertion of BP_{1-2} increased exciton dissociation efficiency from 86% to 98% and higher free carrier density from 1.92×10^{14} cm^{-3} to 2.82×10^{14} cm^{-3} (calculated from Mott–Schottky plots, Fig. 13d). Accordingly, the PCE increased from 10.48% for pristine $CsPbI_3$ devices to 14.17% for $CsPbI_3$–BP devices.[122] The pioneering work that used the dielectric screening effect of BP to enhance exciton dissociation opened up new opportunities for comprehensively capitalizing on the numerous advantages of BP in optoelectronics.

4.6. BP as morphology modifiers

In addition to facilitating carrier transfer, improving light harvest, enhancing exciton dissociation, and constructing heterojunctions for photovoltaics, BP has also been found to effectively modify the morphology of light absorbers in solar cells. BP nanosheets have been reported to improve the molecular ordering and phase purity of the donor:acceptor blend in OSCs *via* π–π interface interactions.[111] Additionally, BPQDs have been observed to serve as heterogeneous nucleation sites in perovskite crystallization.[48,65,123,125] In the following section, recent advances in using BP to modify the morphology of photoabsorbers are scrutinized.

4.6.1 BP as morphology modifiers in OSCs. OSCs can be divided into two categories: whether their acceptors are

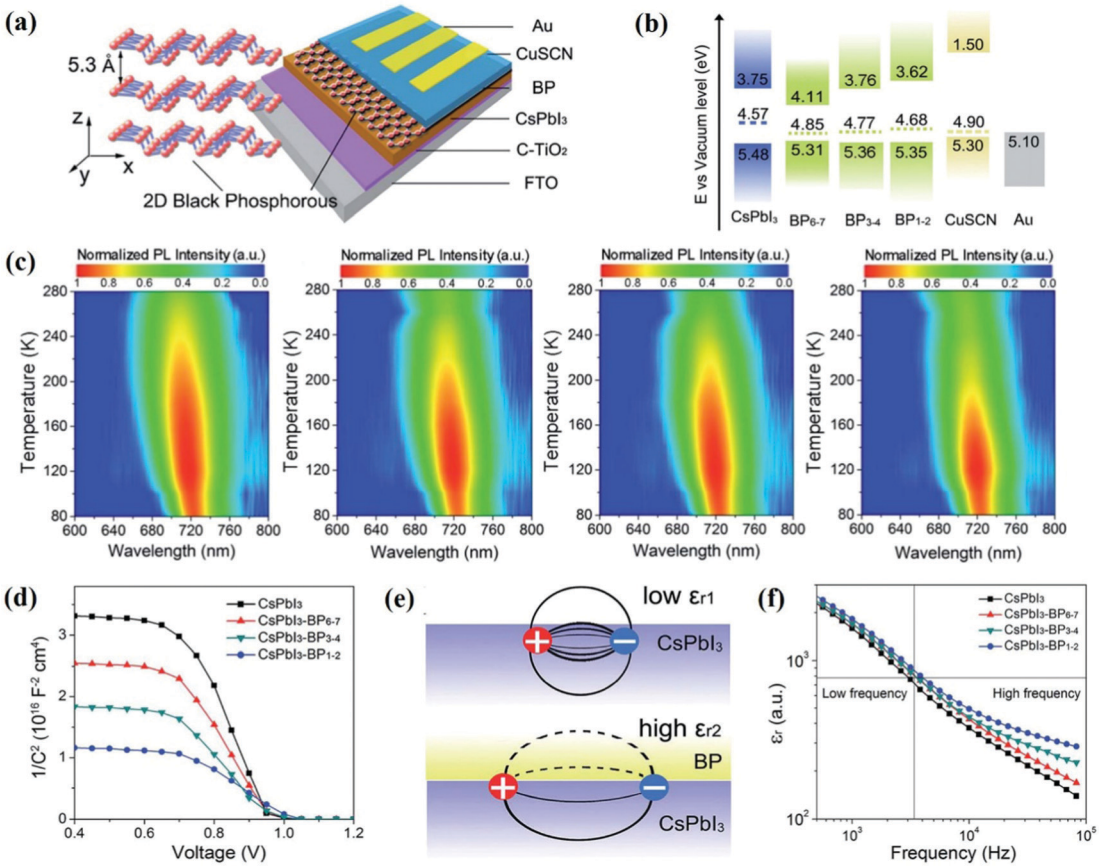

Fig. 13 (a) Schematic of the $CsPbI_3$ solar cell with BP incorporated at the perovskite/HTL interface; (b) energy level diagram; (c) color plots of temperature-dependent PL spectra of pristine $CsPbI_3$, $CsPbI_3$–BP_{6-7}, $CsPbI_3$–BP_{3-4} and $CsPbI_3$–BP_{1-2} heterostructures (from left to right); (d) Mott–Schottky plots; (e) schematic illustration of excitons in different dielectric environments; (f) the real part of the dielectric constant, in which the relative dielectric constant at low frequencies and high frequencies corresponds to the motion dynamics of the charged species at TiO_2/$CsPbI_3$ and $CsPbI_3$/CuSCN interfaces, respectively. Reproduced with permission from ref. 122. Copyright 2019, The Royal Society of Chemistry.

fullerene-based and fullerene-free. In fullerene-free OSCs, the small molecular acceptors tend to mix with donor polymers during OSC fabrication, which has been observed to impede phase separation.[157] The mixed morphology of the donor: acceptor blend without efficient phase separation has been shown to lead to severe charge recombination, poor carrier transport, and thus decreased photovoltaic performance in terms of low FF. 2D materials, such as graphene oxide (GO) and MoS_2, have been reported to enhance the crystalline packing and the optoelectronic properties of conjugated polymers *via* their π–π interface interactions.[158,159] Inspired by this, BP nanosheets with large π-conjugated structures and superior electronic properties were explored as morphology modifiers in fullerene-free OSCs.[111] Particularly, monolayer BP nanoflakes with an average size of 46 nm[111] were prepared to match the domain size in bulk heterojunctions.[160] The incorporation of BP was revealed to obviously enhance the π–π stacking of the blend (Fig. 14d) and slightly enhance the molecular ordering (Fig. 14c) as verified by grazing-incidence wide-angle X-ray scattering (GIWAXS) measurements (Fig. 14a and b). Additionally, increased domain purity in the blend with BP was observed from the increased integrated scattering intensity in the resonant soft X-ray scattering (R-SoXS) profile (Fig. 14e).[111] More ordered π–π stacking, higher molecular ordering, and higher phase purity are desirable for efficient charge transport and suppressing bimolecular recombination in OSCs, which further leads to boosted photovoltaic performance. Furthermore, the morphological stability of the bulk heterojunction was also improved, which was probably due to the space confinement effect of the embedded BP nanoflakes that locked the refined phase separation microstructure.[111] It is worth pointing out that the broad utility of BP as an efficient morphology modifier for fullerene-free OSCs has been demonstrated in two different heterojunctions, *i.e.*, PTB7-Th:IEICO-4F and PBDB-T:ITIC blends.[111]

4.6.2 BP-assisted perovskite growth in PSCs. It has been well documented that the morphology of perovskite films is strongly correlated with their supporting interface. Interfacial application of 2D materials, such as graphene oxide and WS_2 nanosheets, has been reported to result in perovskite films with higher coverage and favorable textures.[161] Similarly, 2D BP-assisted perovskite growth has been observed when BP is incorporated as an interfacial buffer layer for enhanced hole or electron transfer.[46,65,121] He *et al.* first found that BPQDs served as nucleation sites for $MAPbI_3$ crystallization when applied to enhance hole extraction at the anode side in planar PSCs with a p–i–n structure.[65] The incorporation of BPQDs reduced the nuclei density and further led to the growth of large grain size perovskite crystals.[65] Using BP as the ETL or buffer layer at the ETL/perovskite interface in n–i–p structured PSCs has similarly been shown to yield compact perovskite films with a larger grain size, fewer traps and good crystallization.[46,121] In addition to interfacial applications, the compatibility of mixing BP with perovskite precursor solutions to improve film quality has also been demonstrated.[48,123] Yet, in this case, the distribution of BP in perovskite films was reported to be drastically different

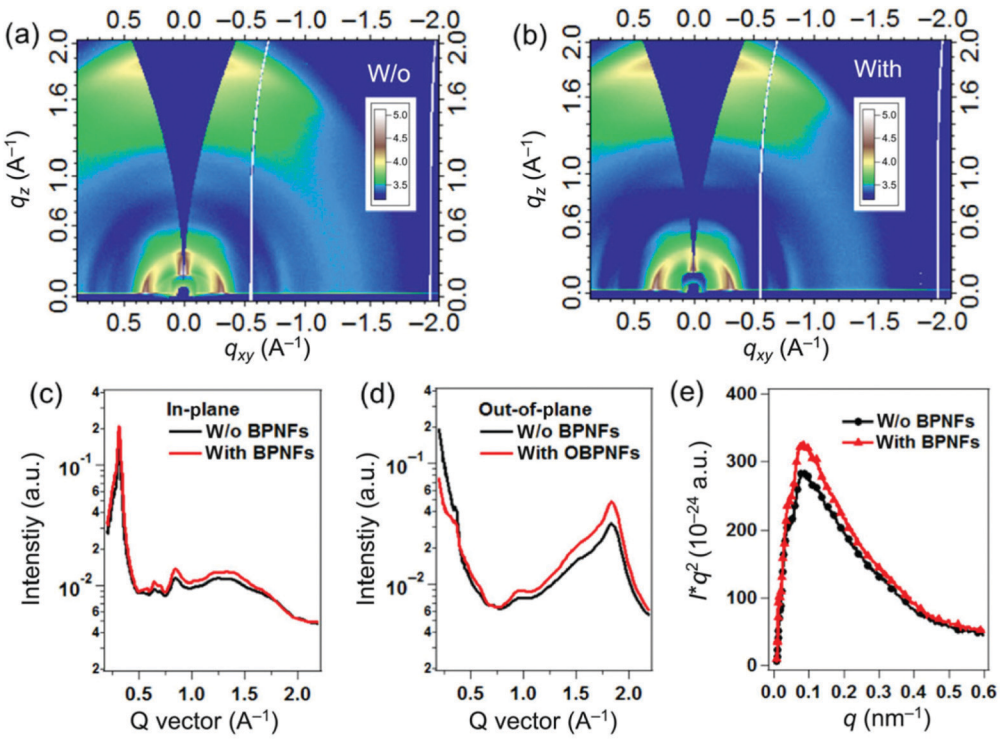

Fig. 14 2D GIWAXS images of PTB7-Th:IEICO-4F blends (a) without and (b) with BP nanoflakes (BPNFs). Intensity profiles *versus* (c) in-plane direction q_{xy} and (d) out-of-plane q_z. (e) Lorentz corrected and thickness normalized R-SoXS profiles of the blend w/wo BPNFs. Reproduced with permission from ref. 111. Copyright 2019, Springer Nature.

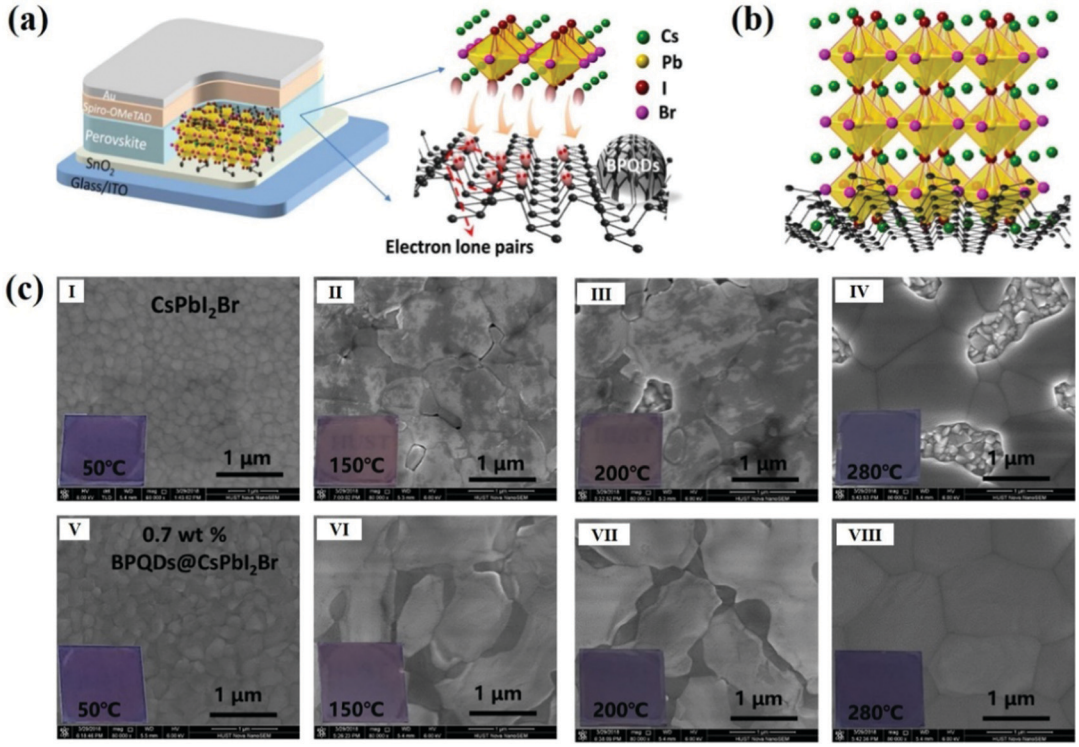

Fig. 15 Schematic structure of (a) the device and interaction between BPQDs and $CsPbI_2Br$, (b) $CsPbI_2Br$ growth on the BPQDs surface; (c) SEM images of the (I–IV) $CsPbI_2Br$ film and (V–VIII) BPQDs@$CsPbI_2Br$ film. Reproduced with permission from ref. 125. Copyright 2020, American Association for the Advancement of Science.

according to the morphology of BP samples. While BPQDs were mainly distributed at the bottom of the perovskite film as heterogeneous nucleation centers,[48] BP flakes with a large lateral size of ~0.5–2 μm were found to be homogeneously distributed in the $MAPbI_3$ perovskite layer,[123] Particularly, BP flakes also functioned as a charge transport mediator in the $MAPbI_3$/BP film.[123] These findings further demonstrate the multiple potential uses of BP in photovoltaic applications.

The dual function of BPQDs in assisting perovskite growth and boosting carrier transport has also been well demonstrated in fully inorganic $CsPbI_2Br$ solar cells.[125] The contributions of BPQDs in modulating the nucleation and crystallization of $CsPbI_2Br$ were revealed in detail in this work. Specifically, the positive Cs^+ cations were able to bind with the lone-pair electrons in the BPQDs (Fig. 15a), and the corner-sharing lead-halide octahedrons then stacked near the surface of the BPQDs to form a hybrid film of BPQDs embedded in a $CsPbI_2Br$ matrix (Fig. 15b). As a result, the as-prepared BPQDs with a narrow size distribution (3–5 nm) served as effective heterogeneous nucleation sites and triggered the uniform growth of $CsPbI_2Br$ crystals. The "BPQD-seeded" growth strategy both improved film morphology and shortened the phase transition period to obtain a pure α-phase $CsPbI_2Br$ (Fig. 15c).[125] In addition, the electronic bonding at the heterojunction hybrid interface between BPQDs and $CsPbI_2Br$ resulted in superior electron-extracting efficiency. The enhanced crystallization and improved carrier transport in BPQD-embedded $CsPbI_2Br$ films boosted the PCE to 15.7% in the corresponding device.[125]

5. Conclusion and outlook

BP is widely recognized as an emerging 2D layered material for diverse optoelectronic applications owing to its compelling semiconductor properties. In this review, the notable attributes of BP, top-down and bottom-up routes to scalable BP preparation, and recent advances in BP-incorporated solar cells are discussed. Nonetheless, considerable efforts are still required to further promote the use of BP for developing high-performance, low-cost third-generation solar cells to compete with commercial Si-based solar cells. To this end, we highlight several scientific and practical challenges and opportunities in order to realise the full potential of BP for constructing high-efficiency solar cells.

(a) Controlled synthesis of monolayer and few-layer BP

Though BP possesses a largely tunable bandgap from 0.3 eV in the bulk to 2.0 eV in the monolayer, it is worth noting that the bandgap of BP experiences a dramatic change from 2.0 eV in the monolayer to ~0.7 eV in five layers.[16,17] As such, it is of great significance to synthesize BP of few-layer thickness in a precisely controllable manner. Currently, BP flakes or QDs for solar cells are nearly all synthesized *via* liquid phase exfoliation, especially ultrasonication-assisted exfoliation (Table 2). However, long processing duration and high sonication energy are necessary in liquid phase exfoliation in order to achieve single-layer or ultra-thin BP. This introduces many structural defects in exfoliated BP, leading to relatively low quality and small lateral size of BP.[3,32,53–56] However, liquid phase

exfoliation synthesis may still dominate in BP production in the near future due to its simplicity, low cost, high throughput and excellent compatibility with device fabrication. In this context, shear-assisted liquid phase exfoliation needs to be promoted as it could efficiently produce ultra-thin BP flakes with uniform size and thickness distribution.[79,162] Regarding bottom-up approaches, efforts to overcome rigorous reaction conditions in pulsed laser deposition of BP are required in the future to render the synthesis compatibility of BP with soft constituents in solar cells.

(b) Investigation into the effect of interlayer interactions on the electronic properties of BP

Though many theoretical investigations on the electronic properties of BP revealed its thickness-dependent electronic band structure, carrier mobility, anisotropic properties, *etc.*, experimental studies on its fundamental properties are relatively few. This is due partially to the lack of well-controlled methods for BP synthesis as well as its stability issue during characterization and measurements. In addition to degradation, crystalline BP is also found to be easily destroyed under an electron beam during imaging, converting into amorphous BP.[44,46] It is noteworthy that fundamental studies on BP properties are readily accessible due to recent advances in BP synthesis and surface passivation techniques.[96] As a result, systematic experimental studies on the thickness-dependent electronic properties of BP are highly feasible, thus providing insight into its various future applications. One crucial yet overlooked issue in the current investigation is the secondary stack of BP flakes during application. Particularly, when applied as thin films in devices, ultra-thin BP samples were usually repeatedly spin-coated to reach a thickness of dozens or even hundreds of nanometers.[116,119–122] Yet, compared to its original dispersed counterpart, electronic properties of such thick BP films resulting from the stacking of thin BP nanosheets have rarely been studied. It remains an open question as to whether or how the secondary stack will affect the electronic properties of the as-exfoliated BP in devices. In this context, it is imperative to *in situ* characterize BP in specific device applications to underpin the improved device performance upon the incorporation of BP.

(c) Meticulous design for rendering dual function or multifunction of BP in solar cells

Regardless of its impressive capability in improving the photovoltaic performance as detailed in Section 4, research in BP-incorporated solar cells is centered primarily on the utility of one function of BP instead of concurrently implementing its multifunctionalities (see Major BP function; Table 2). It is expected that dual functionality or even multifunctionality of BP could be enabled *via* delicate device designs in future studies. Taking an OSC as an example, the thickness of its light absorbing layer is typically limited to approximately 100 nm to ensure efficient carrier transport and collection due to the relatively low carrier mobility of organic semiconductors.[109,110] Clearly, there is a tradeoff between light harvesting and charge transport in OSCs that restricts its efficiency improvement. To this end, the incorporation of BP into organic light absorbers to construct ternary OSCs results in two advantageous aspects, that is, superior carrier transport properties and broad light absorption of BP. In addition, it is amenable for BP to interface closely with either the donor or acceptor *via* convenient tailoring of band alignments. Likewise, BP may also be able to play an essential role in simultaneously assisting perovskite growth, enhancing exciton dissociation, and facilitating charge extraction and transport in PSCs *via* an exquisite device design and BP positioning, as each function of BP has been demonstrated separately in the literature.[46,122,125] Taken together, it is not surprising that the multifunctionality of BP enabled *via* a meticulous design may render fundamental and technological breakthroughs in photovoltaics in the future.

(d) Exploration of BP solar cells

The broad absorption of BP from the visible to the mid-infrared region makes it a promising photoabsorber for constructing solar cells. BPQDs have been explored as the only light absorber in DSSCs.[114] Though the PCE was not satisfying, this pioneering work signifies the potential of exploring BP as the light harvester for solar cells, thus expanding the category of new-generation photovoltaics. Due to its large absorption coefficient and high transparency, BP is well positioned for fabricating semi-transparent solar cells, which can be integrated as windows and skylights towards energy efficient buildings. It is notable that the absorption coefficient of BP is much higher than that of most of the organic semiconductors with the same thickness.[16,163] Promising photovoltaic performance has been predicted in many theoretical studies.[140–146] Specifically, 2D HJSCs with ultrathin thickness composed of a hetero-bilayer or trilayer were able to deliver a high theoretical maximum PCE of ~18–20%, which is extremely competitive over other types of 2D heterojunctions[140,141,145] Likewise, a p–n homojunction diode based on few-layer BP in a lateral structure has been demonstrated, displaying efficient photovoltaic behavior.[164] These pioneering studies suggest considerable opportunities for BP-based 2D HJSCs, which will likely garner much attention from the photovoltaics community in the near future.

(e) Scrutiny of interfacial interaction between BP and other functional layers

To date, analysis on enhanced photovoltaic performance (*e.g.*, improved bandgap alignment, facilitated carrier extraction and transport, and enhanced light absorption) resulting from BP incorporation is mainly concentrated on the intrinsic properties of BP in most of the studies. On the other hand, the interaction between BP and other functional layers in solar cells, such as van der Waals heterojunction,[46] bonding,[125] *etc.*, also plays a vital role in improving the device performance. The sp^3 hybridization in the BP structure leaves behind a lone electron pair pointing out of the layer.[37] Despite the susceptible oxidation of BP due to the presence of the lone electron pair, the latter, on the other hand, provides active sites for BP to interact with other functional materials. As such, increased attention in future studies is expected in this largely overlooked aspect (*i.e.*, the

interaction between BP and other functional layers in solar cells). Clearly, rational design *via* capitalizing on the bonding of BP with the constituents of interest in solar cells merits further exploration to passivate defects, enhance interfacial properties, *etc.* for high device performance.

(f) Functionalization and doping of BP

The thickness-dependent, highly tunable bandgap and electronic properties of BP can be further tailored *via* applying an external electrical field, strain, functionalization, doping, *etc.*[24,25,165] Particularly, the latter two have been demonstrated to be highly effective in concurrently manipulating the electronic properties and stability of BP, making functionalization and doping even more attractive in tuning the electrical properties of BP for various optoelectronic applications.[26,166] For example, the covalent functionalization of BP with aryl diazonium not only yielded a strong p-type doping that simultaneously improved the mobility and on/off current ratio of the resulting field-effect transistor, but also suppressed the chemical degradation of exfoliated BP even after three weeks of ambient exposure.[166] Investigations have shown that the bandgap of BP can be further reduced by alloying arsenic or carbon element.[167,168] The hole mobility of phosphorus carbide was predicted to be several times larger than that of intrinsic BP.[168] It is worth noting that current studies on BP-incorporated solar cells are all centered on pure exfoliated BP without any subsequent chemical modification (Table 2). Thus, future studies on the functionalization and doping of BP are strongly encouraged to further improve its properties, enhance its band structure compatibility with other semiconductors, and broaden its applications.

(g) Device encapsulation for the long-term stability of BP-incorporated solar cells

The major drawback of BP is its instability under ambient conditions. However, its stability is not a great challenge for its application in solar cells, as discussed in Section 2.5. In most of the studies (Table 2), the incorporation of BP as additives or functional layers in solar cells is sheltered by the matrix or sandwiching layers, which protect BP from degradation. Nonetheless, device encapsulation is still important for long-term, practical applications. In future study, the incorporation of BP in solar cells will be further extended to some air-exposed situations, such as being employed as the sole carrier transport layer directly above the perovskite absorber in PSCs[120] or applied as transparent electrodes.[169] In this context, it is necessary to encapsulate devices to ensure their long stability. In addition to encapsulation, other strategies (*e.g.*, covalent[170] and noncovalent functionalization,[171] metal-ion modification,[172] and doping[173]) developed for concurrently regulating the electrical properties of BP and yielding improved stability will also further promote a wide variety of applications of BP.

Conflicts of interest

There are no conflicts to declare.

Acknowledgements

This work was supported by the NSF (CMMI 1914713, ECCS 1914562, DMR 1903990).

References

1 A. Carvalho, M. Wang, X. Zhu, A. S. Rodin, H. Su and A. H. Castro Neto, *Nat. Rev. Mater.*, 2016, **1**, 16061.
2 L. Li, Y. Yu, G. J. Ye, Q. Ge, X. Ou, H. Wu, D. Feng, X. H. Chen and Y. Zhang, *Nat. Nanotechnol.*, 2014, **9**, 372.
3 J. R. Brent, N. Savjani, E. A. Lewis, S. J. Haigh, D. J. Lewis and P. O'Brien, *Chem. Commun.*, 2014, **50**, 13338–13341.
4 L. Liang, J. Wang, W. Lin, B. G. Sumpter, V. Meunier and M. Pan, *Nano Lett.*, 2014, **14**, 6400–6406.
5 M. Batmunkh, M. Bat-Erdene and J. G. Shapter, *Adv. Energy Mater.*, 2018, **8**, 1701832.
6 J. Pang, A. Bachmatiuk, Y. Yin, B. Trzebicka, L. Zhao, L. Fu, R. G. Mendes, T. Gemming, Z. Liu and M. H. Rummeli, *Adv. Energy Mater.*, 2018, **8**, 1702093.
7 J. Liu, Y. Yao, S. Xiao and X. Gu, *J. Phys. D: Appl. Phys.*, 2018, **51**, 123001.
8 C. Battaglia, A. Cuevas and S. De Wolf, *Energy Environ. Sci.*, 2016, **9**, 1552–1576.
9 N. R. E. L. (Nrel), Best Research-Cell Efficiency Chart (2021), https://www.nrel.gov/pv/cell-efficiency.html.
10 B. Wang, J. Iocozzia, M. Zhang, M. Ye, S. Yan, H. Jin, S. Wang, Z. Zou and Z. Lin, *Chem. Soc. Rev.*, 2019, **48**, 4854–4891.
11 P. Bridgman, *J. Am. Chem. Soc.*, 1914, **36**, 1344–1363.
12 H. Du, X. Lin, Z. Xu and D. Chu, *J. Mater. Chem. C*, 2015, **3**, 8760–8775.
13 M. Akhtar, G. Anderson, R. Zhao, A. Alruqi, J. E. Mroczkowska, G. Sumanasekera and J. B. Jasinski, *npj 2D Mater. Appl.*, 2017, **1**, 1–13.
14 H. Liu, A. T. Neal, Z. Zhu, Z. Luo, X. Xu, D. Tománek and P. D. Ye, *ACS Nano*, 2014, **8**, 4033–4041.
15 M. Batmunkh, M. Bat-Erdene and J. G. Shapter, *Adv. Mater.*, 2016, **28**, 8586–8617.
16 V. Tran, R. Soklaski, Y. Liang and L. Yang, *Phys. Rev. B: Condens. Matter Mater. Phys.*, 2014, **89**, 235319.
17 A. Castellanos-Gomez, *J. Phys. Chem. Lett.*, 2015, **6**, 4280–4291.
18 H. Yuan, X. Liu, F. Afshinmanesh, W. Li, G. Xu, J. Sun, B. Lian, A. G. Curto, G. Ye and Y. Hikita, *Nat. Nanotechnol.*, 2015, **10**, 707.
19 Z. S. Popović, J. M. Kurdestany and S. Satpathy, *Phys. Rev. B: Condens. Matter Mater. Phys.*, 2015, **92**, 035135.
20 S. Lin, Y. Chui, Y. Li and S. P. Lau, *FlatChem*, 2017, **2**, 15–37.
21 Y. Takao, H. Asahina and A. Morita, *J. Phys. Soc. Jpn.*, 1981, **50**, 3362–3369.
22 S. Lin, Y. Li, J. Qian and S. P. Lau, *Mater. Today Energy*, 2019, **12**, 1–25.
23 J. Qiao, X. Kong, Z.-X. Hu, F. Yang and W. Ji, 2014, arXiv preprint arXiv:1401.5045.

24 B. Deng, V. Tran, Y. Xie, H. Jiang, C. Li, Q. Guo, X. Wang, H. Tian, S. J. Koester and H. Wang, *Nat. Commun.*, 2017, **8**, 14474.
25 J. Kim, S. S. Baik, S. H. Ryu, Y. Sohn, S. Park, B.-G. Park, J. Denlinger, Y. Yi, H. J. Choi and K. S. Kim, *Science*, 2015, **349**, 723–726.
26 S. P. Koenig, R. A. Doganov, L. Seixas, A. Carvalho, J. Y. Tan, K. Watanabe, T. Taniguchi, N. Yakovlev, A. H. Castro Neto and B. Ozyilmaz, *Nano Lett.*, 2016, **16**, 2145–2151.
27 Y. Cai, G. Zhang and Y.-W. Zhang, *Sci. Rep.*, 2014, **4**, 6677.
28 R. W. Keyes, *Phys. Rev.*, 1953, **92**, 580.
29 L. Li, Y. Yu, G. J. Ye, Q. Ge, X. Ou, H. Wu, D. Feng, X. H. Chen and Y. Zhang, *Nat. Nanotechnol.*, 2014, **9**, 372.
30 J. Qiao, X. Kong, Z.-X. Hu, F. Yang and W. Ji, *Nat. Commun.*, 2014, **5**, 4475.
31 R. Fei and L. Yang, *Nano Lett.*, 2014, **14**, 2884–2889.
32 P. Yasaei, B. Kumar, T. Foroozan, C. Wang, M. Asadi, D. Tuschel, J. E. Indacochea, R. F. Klie and A. Salehi-Khojin, *Adv. Mater.*, 2015, **27**, 1887–1892.
33 M. Z. Rahman, C. W. Kwong, K. Davey and S. Z. Qiao, *Energy Environ. Sci.*, 2016, **9**, 709–728.
34 J.-H. Lin, H. Zhang and X.-L. Cheng, *Front. Phys.*, 2015, **10**, 1–9.
35 J. He, D. He, Y. Wang, Q. Cui, M. Z. Bellus, H.-Y. Chiu and H. Zhao, *ACS Nano*, 2015, **9**, 6436–6442.
36 D. Çakır, H. Sahin and F. M. Peeters, *Phys. Rev. B: Condens. Matter Mater. Phys.*, 2014, **90**, 205421.
37 A. Ziletti, A. Carvalho, D. K. Campbell, D. F. Coker and A. C. Neto, *Phys. Rev. Lett.*, 2015, **114**, 046801.
38 J. Lu, J. Wu, A. Carvalho, A. Ziletti, H. Liu, J. Tan, Y. Chen, A. Castro Neto, B. Ozyilmaz and C. H. Sow, *ACS Nano*, 2015, **9**, 10411–10421.
39 A. Favron, E. Gaufrès, F. Fossard, A.-L. Phaneuf-L'Heureux, N. Y. Tang, P. L. Lévesque, A. Loiseau, R. Leonelli, S. Francoeur and R. Martel, *Nat. Mater.*, 2015, **14**, 826.
40 J. D. Wood, S. A. Wells, D. Jariwala, K.-S. Chen, E. Cho, V. K. Sangwan, X. Liu, L. J. Lauhon, T. J. Marks and M. C. Hersam, *Nano Lett.*, 2014, **14**, 6964–6970.
41 A. Avsar, I. J. Vera-Marun, J. Y. Tan, K. Watanabe, T. Taniguchi, A. H. Castro Neto and B. Ozyilmaz, *ACS Nano*, 2015, **9**, 4138–4145.
42 G. C. Constantinescu and N. D. Hine, *Nano Lett.*, 2016, **16**, 2586–2594.
43 Y. Cai, G. Zhang and Y.-W. Zhang, *J. Phys. Chem. C*, 2015, **119**, 13929–13936.
44 Z. Guo, H. Zhang, S. Lu, Z. Wang, S. Tang, J. Shao, Z. Sun, H. Xie, H. Wang and X. F. Yu, *Adv. Funct. Mater.*, 2015, **25**, 6996–7002.
45 D. Hanlon, C. Backes, E. Doherty, C. S. Cucinotta, N. C. Berner, C. Boland, K. Lee, A. Harvey, P. Lynch and Z. Gholamvand, *Nat. Commun.*, 2015, **6**, 8563.
46 M. Zhang, M. Ye, W. Wang, C. Ma, S. Wang, Q. Liu, T. Lian, J. Huang and Z. Lin, *Adv. Mater.*, 2020, 2000999.
47 W. Dong, S. Xiong, J. Yang, W. Qiao, Q. Zeng, X. Wang, Y. Yao and Q. Bao, *Org. Electron.*, 2021, **89**, 106052.
48 W. Yang, J. Chen, X. Lian, J. Li, F. Yao, G. Wu, W. Qiu, C. Jin, P. Heremans and H. Chen, *Solar RRL*, 2019, **3**, 1900132.
49 D. K. Sang, H. Wang, Z. Guo, N. Xie and H. Zhang, *Adv. Funct. Mater.*, 2019, **29**, 1903419.
50 J. Jia, S. K. Jang, S. Lai, J. Xu, Y. J. Choi, J.-H. Park and S. Lee, *ACS Nano*, 2015, **9**, 8729–8736.
51 Y. Xu, X. Shi, Y. Zhang, H. Zhang, Q. Zhang, Z. Huang, X. Xu, J. Guo, H. Zhang and L. Sun, *Nat. Commun.*, 2020, **11**, 1–8.
52 D. Hanlon, C. Backes, E. Doherty, C. S. Cucinotta, N. C. Berner, C. Boland, K. Lee, A. Harvey, P. Lynch and Z. Gholamvand, *Nat. Commun.*, 2015, **6**, 1–11.
53 J. Kang, J. D. Wood, S. A. Wells, J.-H. Lee, X. Liu, K.-S. Chen and M. C. Hersam, *ACS Nano*, 2015, **9**, 3596–3604.
54 M. Qiu, D. Wang, W. Liang, L. Liu, Y. Zhang, X. Chen, D. K. Sang, C. Xing, Z. Li and B. Dong, *Proc. Natl. Acad. Sci. U. S. A.*, 2018, **115**, 501–506.
55 J. Gómez-Pérez, Z. Kónya and Á. Kukovecz, *Nanotechnology*, 2018, **29**, 365303.
56 G. Abellán, V. Lloret, U. Mundloch, M. Marcia, C. Neiss, A. Görling, M. Varela, F. Hauke and A. Hirsch, *Angew. Chem., Int. Ed.*, 2016, **128**, 14777–14782.
57 J. Kang, S. A. Wells, J. D. Wood, J.-H. Lee, X. Liu, C. R. Ryder, J. Zhu, J. R. Guest, C. A. Husko and M. C. Hersam, *Proc. Natl. Acad. Sci. U. S. A.*, 2016, **113**, 11688–11693.
58 L. Chen, G. Zhou, Z. Liu, X. Ma, J. Chen, Z. Zhang, X. Ma, F. Li, H. M. Cheng and W. Ren, *Adv. Mater.*, 2016, **28**, 510–517.
59 M. Lee, A. K. Roy, S. Jo, Y. Choi, A. Chae, B. Kim, S. Y. Park and I. In, *Nanotechnology*, 2017, **28**, 125603.
60 W. Liu, Y. Zhu, Z. Chen, J. Lei and P. Feng, *J. Electron. Mater.*, 2018, **47**, 4793–4798.
61 L.-F. Gao, J.-Y. Xu, Z.-Y. Zhu, C.-X. Hu, L. Zhang, Q. Wang and H.-L. Zhang, *Nanoscale*, 2016, **8**, 15132–15136.
62 J.-Y. Xu, L.-F. Gao, C.-X. Hu, Z.-Y. Zhu, M. Zhao, Q. Wang and H.-L. Zhang, *Chem. Commun.*, 2016, **52**, 8107–8110.
63 Q. Zhang, S. Huang, J. Deng, D. T. Gangadharan, F. Yang, Z. Xu, G. Giorgi, M. Palummo, M. Chaker and D. Ma, *Adv. Funct. Mater.*, 2019, **29**, 1902486.
64 X. Zhang, H. Xie, Z. Liu, C. Tan, Z. Luo, H. Li, J. Lin, L. Sun, W. Chen and Z. Xu, *Angew. Chem., Int. Ed.*, 2015, **54**, 3653–3657.
65 W. Chen, K. Li, Y. Wang, X. Feng, Z. Liao, Q. Su, X. Lin and Z. He, *J. Phys. Chem. Lett.*, 2017, **8**, 591–598.
66 R. Meng, J. Huang, Y. Feng, L. Zu, C. Peng, L. Zheng, L. Zheng, Z. Chen, G. Liu and B. Chen, *Adv. Energy Mater.*, 2018, **8**, 1801514.
67 Z. Sun, H. Xie, S. Tang, X. F. Yu, Z. Guo, J. Shao, H. Zhang, H. Huang, H. Wang and P. K. Chu, *Angew. Chem., Int. Ed.*, 2015, **54**, 11526–11530.
68 A. Ambrosi, Z. Sofer and M. Pumera, *Angew. Chem., Int. Ed.*, 2017, **129**, 10579–10581.
69 H. Xiao, M. Zhao, J. Zhang, X. Ma, J. Zhang, T. Hu, T. Tang, J. Jia and H. Wu, *Electrochem. Commun.*, 2018, **89**, 10–13.

70 J. Li, C. Chen, S. Liu, J. Lu, W. P. Goh, H. Fang, Z. Qiu, B. Tian, Z. Chen and C. Yao, *Chem. Mater.*, 2018, **30**, 2742–2749.
71 F. Luo, D. Wang, J. Zhang, X. Li, D. Liu, H. Li, M. Lu, X. Xie, L. Huang and W. Huang, *ACS Appl. Nano Mater.*, 2019, **2**, 3793–3801.
72 E. Kovalska, J. Luxa, T. Hartman, N. Antonatos, P. Shaban, E. Oparin, M. Zhukova and Z. Sofer, *Nanoscale*, 2020, **12**, 2638–2647.
73 T. Liang, Y. Liu, P. Zhang, C. Liu, F. Ma, Q. Yan and Z. Dai, *Chem. Eng. J.*, 2020, **395**, 124976.
74 E. Kovalska, J. Luxa, M. Melle-Franco, B. Wu, I. Marek, P. K. Roy, P. Marvan and Z. Sofer, *ACS Appl. Mater. Interfaces*, 2020, **12**, 50516–50526.
75 S. Qiu, B. Zou, H. Sheng, W. Guo, J. Wang, Y. Zhao, W. Wang, R. K. Yuen, Y. Kan and Y. Hu, *ACS Appl. Mater. Interfaces*, 2019, **11**, 13652–13664.
76 M. O. Valappil, M. Ahlawat, V. K. Pillai and S. Alwarappan, *Chem. Commun.*, 2018, **54**, 11733–11736.
77 M. Ozhukil Valappil, K. Joshi, L. John, S. Krishnamurthy, B. Jana, A. Patra, V. K. Pillai and S. Alwarappan, *J. Phys. Chem. Lett.*, 2019, **10**, 973–980.
78 Z. Liu, Y. Sun, H. Cao, D. Xie, W. Li, J. Wang and A. K. Cheetham, *Nat. Commun.*, 2020, **11**, 1–10.
79 F. Xu, H. Ma, S. Lei, J. Sun, J. Chen, B. Ge, Y. Zhu and L. Sun, *Nanoscale*, 2016, **8**, 13603–13610.
80 M. Batmunkh, K. Vimalanathan, C. Wu, A. S. Bati, L. Yu, S. A. Tawfik, M. J. Ford, T. J. Macdonald, C. L. Raston and S. Priya, *Small Methods*, 2019, **3**, 1800521.
81 F. Xu, B. Ge, J. Chen, A. Nathan, L. L. Xin, H. Ma, H. Min, C. Zhu, W. Xia and Z. Li, *2D Mater.*, 2016, **3**, 025005.
82 C. Zhu, F. Xu, L. Zhang, M. Li, J. Chen, S. Xu, G. Huang, W. Chen and L. Sun, *Chem. – Eur. J.*, 2016, **22**, 7357–7362.
83 Z. Yan, X. He, L. She, J. Sun, R. Jiang, H. Xu, F. Shi, Z. Lei and Z.-H. Liu, *J. Materiomics*, 2018, **4**, 129–134.
84 W. Gu, X. Pei, Y. Cheng, C. Zhang, J. Zhang, Y. Yan, C. Ding and Y. Xian, *ACS Sens.*, 2017, **2**, 576–582.
85 Z. Wang, Y. Xu, S. C. Dhanabalan, J. Sophia, C. Zhao, C. Xu, Y. Xiang, J. Li and H. Zhang, *IEEE Photonics J.*, 2016, **8**, 1–10.
86 Y. Xu, Z. Wang, Z. Guo, H. Huang, Q. Xiao, H. Zhang and X. F. Yu, *Adv. Opt. Mater.*, 2016, **4**, 1223–1229.
87 M. Batmunkh, A. Shrestha, M. Bat-Erdene, M. J. Nine, C. J. Shearer, C. T. Gibson, A. D. Slattery, S. A. Tawfik, M. J. Ford and S. Dai, *Angew. Chem., Int. Ed.*, 2018, **57**, 2644–2647.
88 M. Bat-Erdene, M. Batmunkh, C. J. Shearer, S. A. Tawfik, M. J. Ford, L. Yu, A. J. Sibley, A. D. Slattery, J. S. Quinton and C. T. Gibson, *Small Methods*, 2017, **1**, 1700260.
89 K. Du, W. Yang, S. Deng, X. Li and P. Yang, *Nanomaterials*, 2020, **10**, 139.
90 M. Batmunkh, M. Myekhlai, A. S. Bati, S. Sahlos, A. D. Slattery, T. M. Benedetti, V. R. Gonçales, C. T. Gibson, J. J. Gooding and R. D. Tilley, *J. Mater. Chem. A*, 2019, **7**, 12974–12978.
91 X. Zhu, T. Zhang, Z. Sun, H. Chen, J. Guan, X. Chen, H. Ji, P. Du and S. Yang, *Adv. Mater.*, 2017, **29**, 1605776.
92 Z. Sofer, D. Bouša, J. Luxa, V. Mazanek and M. Pumera, *Chem. Commun.*, 2016, **52**, 1563–1566.
93 X. Ren, X. Yang, G. Xie and J. Luo, *ACS Appl. Nano Mater.*, 2020, **3**, 4799–4809.
94 C. Sun, L. Wen, J. Zeng, Y. Wang, Q. Sun, L. Deng, C. Zhao and Z. Li, *Biomaterials*, 2016, **91**, 81–89.
95 A. Khandelwal, K. Mani, M. H. Karigerasi and I. Lahiri, *Mater. Sci. Eng., B*, 2017, **221**, 17–34.
96 Z. Wu, Y. Lyu, Y. Zhang, R. Ding, B. Zheng, Z. Yang, S. P. Lau, X. H. Chen and J. Hao, *Nat. Mater.*, 2021, 1–7.
97 B. Tian, B. Tian, B. Smith, M. Scott, R. Hua, Q. Lei and Y. Tian, *Nat. Commun.*, 2018, **9**, 1–11.
98 X. Li, B. Deng, X. Wang, S. Chen, M. Vaisman, S.-I. Karato, G. Pan, M. L. Lee, J. Cha and H. Wang, *2D Mater.*, 2015, **2**, 031002.
99 J. B. Smith, D. Hagaman and H.-F. Ji, *Nanotechnology*, 2016, **27**, 215602.
100 C. Li, Y. Wu, B. Deng, Y. Xie, Q. Guo, S. Yuan, X. Chen, M. Bhuiyan, Z. Wu and K. Watanabe, *Adv. Mater.*, 2018, **30**, 1703748.
101 Q. Jiang, L. Xu, N. Chen, H. Zhang, L. Dai and S. Wang, *Angew. Chem., Int. Ed.*, 2016, **128**, 14053–14057.
102 M. Rajabali and S. Mohajerzadeh, *Phys. Status Solidi RRL*, 2019, **13**, 1900197.
103 M. Rajabali, M. Esfandiari, S. Rajabali, M. Vakili-Tabatabaei, S. Mohajerzadeh and S. Mohajerzadeh, *Adv. Mater. Interfaces*, 2020, **7**, 2000774.
104 Z. Yang, J. Hao, S. Yuan, S. Lin, H. M. Yau, J. Dai and S. P. Lau, *Adv. Mater.*, 2015, **27**, 3748–3754.
105 M. Z. Bellus, Z. Yang, P. Zereshki, J. Hao, S. P. Lau and H. Zhao, *Nanoscale Horiz.*, 2019, **4**, 236–242.
106 G. Zhao, T. Wang, Y. Shao, Y. Wu, B. Huang and X. Hao, *Small*, 2017, **13**, 1602243.
107 B. Tian, B. Tian, B. Smith, M. Scott, Q. Lei, R. Hua, Y. Tian and Y. Liu, *Proc. Natl. Acad. Sci. U. S. A.*, 2018, **115**, 4345–4350.
108 S. Lin, S. Liu, Z. Yang, Y. Li, T. W. Ng, Z. Xu, Q. Bao, J. Hao, C. S. Lee and C. Surya, *Adv. Funct. Mater.*, 2016, **26**, 864–871.
109 S. Liu, S. Lin, P. You, C. Surya, S. P. Lau and F. Yan, *Angew. Chem., Int. Ed.*, 2017, **56**, 13717–13721.
110 Y. Zhao, T. L. Chen, L. Xiao, M. A. Kolaczkowski, L. Zhang, L. M. Klivansky, V. Altoe, B. Tian, J. Guo and X. Peng, *Nano Energy*, 2018, **53**, 345–353.
111 W. Yang, L. Ye, F. Yao, C. Jin, H. Ade and H. Chen, *Nano Res.*, 2019, **12**, 777–783.
112 Y. Yang, J. Gao, Z. Zhang, S. Xiao, H. H. Xie, Z. B. Sun, J. H. Wang, C. H. Zhou, Y. W. Wang and X. Y. Guo, *Adv. Mater.*, 2016, **28**, 8937–8944.
113 J. Song, J. Wang, X. Lin, J. He, H. Liu, Y. Lei and Z. Chu, *ChemElectroChem*, 2017, **4**, 2373–2377.
114 H. Yuan, Y. Zhao, Y. Wang, J. Duan, B. He and Q. Tang, *J. Power Sources*, 2019, **410**, 53–58.
115 Y. Xu, X. Wang, M. Jin, G. Zhou and L. Shui, *J. Mater. Sci.*, 2020, **55**, 5499–5509.
116 L. Bai, L. Sun, Y. Wang, Z. Liu, Q. Gao, H. Xiang, H. Xie and Y. Zhao, *J. Mater. Chem. A*, 2017, **5**, 8280–8286.

117 Z. Xia, P. Li, Y. Liu, T. Song, Q. Bao, S.-T. Lee and B. Sun, *Nano Res.*, 2017, **10**, 3848–3856.
118 M. Bat-Erdene, M. Batmunkh, S. A. Tawfik, M. Fronzi, M. J. Ford, C. J. Shearer, L. Yu, M. Dadkhah, J. R. Gascooke and C. T. Gibson, *Adv. Funct. Mater.*, 2017, **27**, 1704488.
119 Q. Li, J. Yang, C. Huang, S. Zeng, J. Zou, X. Zeng, X. Li and Q. Fu, *Mater. Lett.*, 2018, **217**, 92–95.
120 S. K. Muduli, E. Varrla, S. A. Kulkarni, G. Han, K. Thirumal, O. Lev, S. Mhaisalkar and N. Mathews, *J. Power Sources*, 2017, **371**, 156–161.
121 N. Fu, C. Huang, P. Lin, M. Zhu, T. Li, M. Ye, S. Lin, G. Zhang, J. Du and C. Liu, *J. Mater. Chem. A*, 2018, **6**, 8886–8894.
122 B. Li, Y. Zhang, L. Fu, L. Zhang, Z. Liu and L. Yin, *J. Mater. Chem. A*, 2019, **7**, 22539–22549.
123 Y. Wang, H. Zhang, T. Zhang, W. Shi, M. Kan, J. Chen and Y. Zhao, *Solar RRL*, 2019, **3**, 1900197.
124 X. Lin, P.-P. Cheng, Y.-W. Zhang, W.-Y. Tan, D. Yu, G. Yi and Y. Min, *Sol. Energy*, 2020, **206**, 793–798.
125 X. Gong, L. Guan, Q. Li, Y. Li, T. Zhang, H. Pan, Q. Sun, Y. Shen, C. Grätzel and S. M. Zakeeruddin, *Sci. Adv.*, 2020, **6**, eaay5661.
126 O. Malinkiewicz, A. Yella, Y. H. Lee, G. M. Espallargas, M. Graetzel, M. K. Nazeeruddin and H. J. Bolink, *Nat. Photonics*, 2014, **8**, 128.
127 C. Wehrenfennig, G. E. Eperon, M. B. Johnston, H. J. Snaith and L. M. Herz, *Adv. Mater.*, 2014, **26**, 1584–1589.
128 J. Zhang, H. S. Tan, X. Guo, A. Facchetti and H. Yan, *Nat. Energy*, 2018, **3**, 720–731.
129 X. Li, Z. Lv and H. Zhu, *Adv. Mater.*, 2015, **27**, 6549–6574.
130 X.-G. Hu, P.-X. Hou, J.-B. Wu, X. Li, J. Luan, C. Liu, G. Liu and H.-M. Cheng, *Nano Energy*, 2020, **69**, 104442.
131 M. Zhang, X. Cui, Y. Wang, B. Wang, M. Ye, W. Wang, C. Ma and Z. Lin, *Nano Energy*, 2020, **71**, 104620.
132 Q. Dong, Y. Shi, K. Wang, Y. Li, S. Wang, H. Zhang, Y. Xing, Y. Du, X. Bai and T. Ma, *J. Phys. Chem. C*, 2015, **119**, 10212–10217.
133 S.-Y. Tai, C.-J. Liu, S.-W. Chou, F. S.-S. Chien, J.-Y. Lin and T.-W. Lin, *J. Mater. Chem.*, 2012, **22**, 24753–24759.
134 J. He, P. Gao, M. Liao, X. Yang, Z. Ying, S. Zhou, J. Ye and Y. Cui, *ACS Nano*, 2015, **9**, 6522–6531.
135 D. Li, H. Jussila, L. Karvonen, G. Ye, H. Lipsanen, X. Chen and Z. Sun, *Sci. Rep.*, 2015, **5**, 1–9.
136 A. N. Rudenko and M. I. Katsnelson, *Phys. Rev. B: Condens. Matter Mater. Phys.*, 2014, **89**, 201408.
137 X. Li, W. C. Choy, L. Huo, F. Xie, W. E. Sha, B. Ding, X. Guo, Y. Li, J. Hou and J. You, *Adv. Mater.*, 2012, **24**, 3046–3052.
138 S. Liu, P. You, J. Li, J. Li, C.-S. Lee, B. S. Ong, C. Surya and F. Yan, *Energy Environ. Sci.*, 2015, **8**, 1463–1470.
139 D. J. Yang, Y. H. Du, Y. Q. Zhao, Z. L. Yu and M. Q. Cai, *Phys. Status Solidi B*, 2019, **256**, 1800540.
140 H. Guo, N. Lu, J. Dai, X. Wu and X. C. Zeng, *J. Phys. Chem. C*, 2014, **118**, 14051–14059.
141 J. Dai and X. C. Zeng, *J. Phys. Chem. Lett.*, 2014, **5**, 1289–1293.
142 V. D. S. O. Ganesan, J. Linghu, C. Zhang, Y. P. Feng and L. Shen, *Appl. Phys. Lett.*, 2016, **108**, 122105.
143 M. Xie, S. Zhang, B. Cai, Y. Huang, Y. Zou, B. Guo, Y. Gu and H. Zeng, *Nano Energy*, 2016, **28**, 433–439.
144 M. Buscema, D. J. Groenendijk, G. A. Steele, H. S. Van Der Zant and A. Castellanos-Gomez, *Nat. Commun.*, 2014, **5**, 1–6.
145 W. Hu, L. Lin, C. Yang, J. Dai and J. Yang, *Nano Lett.*, 2016, **16**, 1675–1682.
146 M. Kar, R. Sarkar, S. Pal and P. Sarkar, *J. Phys. Chem. C*, 2019, **123**, 20748–20756.
147 J. Shi, H. Zhang, Y. Li, J. J. Jasieniak, Y. Li, H. Wu, Y. Luo, D. Li and Q. Meng, *Energy Environ. Sci.*, 2018, **11**, 1460–1469.
148 J.-C. Blancon, H. Tsai, W. Nie, C. C. Stoumpos, L. Pedesseau, C. Katan, M. Kepenekian, C. M. M. Soe, K. Appavoo and M. Y. Sfeir, *Science*, 2017, **355**, 1288–1292.
149 Q. Lin, A. Armin, R. C. R. Nagiri, P. L. Burn and P. Meredith, *Nat. Photonics*, 2015, **9**, 106–112.
150 Y. Yang, D. P. Ostrowski, R. M. France, K. Zhu, J. Van De Lagemaat, J. M. Luther and M. C. Beard, *Nat. Photonics*, 2016, **10**, 53–59.
151 A. Miyata, A. Mitioglu, P. Plochocka, O. Portugall, J. T.-W. Wang, S. D. Stranks, H. J. Snaith and R. J. Nicholas, *Nat. Phys.*, 2015, **11**, 582–587.
152 C. Wu, Y. Zou, T. Wu, M. Ban, V. Pecunia, Y. Han, Q. Liu, T. Song, S. Duhm and B. Sun, *Adv. Funct. Mater.*, 2017, **27**, 1700338.
153 C. Ma, Y. Shi, W. Hu, M. H. Chiu, Z. Liu, A. Bera, F. Li, H. Wang, L. J. Li and T. Wu, *Adv. Mater.*, 2016, **28**, 3683–3689.
154 R. Ahmad, R. Srivastava, S. Yadav, S. Chand and S. Sapra, *ACS Appl. Mater. Interfaces*, 2017, **9**, 34111–34121.
155 T. Low, R. Roldán, H. Wang, F. Xia, P. Avouris, L. M. Moreno and F. Guinea, *Phys. Rev. Lett.*, 2014, **113**, 106802.
156 A. Raja, A. Chaves, J. Yu, G. Arefe, H. M. Hill, A. F. Rigosi, T. C. Berkelbach, P. Nagler, C. Schüller and T. Korn, *Nat. Commun.*, 2017, **8**, 1–7.
157 J. Hou, O. Inganäs, R. H. Friend and F. Gao, *Nat. Mater.*, 2018, **17**, 119–128.
158 E. Istif, J. Hernández-Ferrer, E. P. Urriolabeitia, A. Stergiou, N. Tagmatarchis, G. Fratta, M. J. Large, A. B. Dalton, A. M. Benito and W. K. Maser, *Adv. Funct. Mater.*, 2018, **28**, 1707548.
159 Y. Zhang, S. Liu, W. Liu, T. Liang, X. Yang, M. Xu and H. Chen, *Phys. Chem. Chem. Phys.*, 2015, **17**, 27565–27572.
160 G. Kakavelakis, A. E. Del Rio Castillo, V. Pellegrini, A. Ansaldo, P. Tzourmpakis, R. Brescia, M. Prato, E. Stratakis, E. Kymakis and F. Bonaccorso, *ACS Nano*, 2017, **11**, 3517–3531.
161 Q. Zhou, J. Duan, X. Yang, Y. Duan and Q. Tang, *Angew. Chem., Int. Ed.*, 2020, **132**, 22181–22185.
162 G. Xing, N. Mathews, S. Sun, S. S. Lim, Y. M. Lam, M. Grätzel, S. Mhaisalkar and T. C. Sum, *Science*, 2013, **342**, 344–347.

163 Z. Liu, S. P. Lau and F. Yan, *Chem. Soc. Rev.*, 2015, **44**, 5638–5679.
164 Y. Liu, Y. Cai, G. Zhang, Y.-W. Zhang and K.-W. Ang, *Adv. Funct. Mater.*, 2017, **27**, 1604638.
165 X. Peng, Q. Wei and A. Copple, *Phys. Rev. B: Condens. Matter Mater. Phys.*, 2014, **90**, 085402.
166 C. R. Ryder, J. D. Wood, S. A. Wells, Y. Yang, D. Jariwala, T. J. Marks, G. C. Schatz and M. C. Hersam, *Nat. Chem.*, 2016, **8**, 597–602.
167 B. Liu, M. Köpf, A. N. Abbas, X. Wang, Q. Guo, Y. Jia, F. Xia, R. Weihrich, F. Bachhuber and F. Pielnhofer, *Adv. Mater.*, 2015, **27**, 4423–4429.
168 W. C. Tan, Y. Cai, R. J. Ng, L. Huang, X. Feng, G. Zhang, Y. W. Zhang, C. A. Nijhuis, X. Liu and K. W. Ang, *Adv. Mater.*, 2017, **29**, 1700503.
169 R. Mehta, M. Min and A. B. Kaul, *J. Vac. Sci. Technol., B: Nanotechnol. Microelectron.: Mater., Process., Meas., Phenom.*, 2020, **38**, 063203.
170 Y. Liu, P. Gao, T. Zhang, X. Zhu, M. Zhang, M. Chen, P. Du, G. W. Wang, H. Ji and J. Yang, *Angew. Chem., Int. Ed.*, 2019, **58**, 1479–1483.
171 R. Gusmão, Z. k. Sofer and M. Pumera, *ACS Nano*, 2018, **12**, 5666–5673.
172 Z. Guo, S. Chen, Z. Wang, Z. Yang, F. Liu, Y. Xu, J. Wang, Y. Yi, H. Zhang and L. Liao, *Adv. Mater.*, 2017, **29**, 1703811.
173 B. Yang, B. Wan, Q. Zhou, Y. Wang, W. Hu, W. Lv, Q. Chen, Z. Zeng, F. Wen and J. Xiang, *Adv. Mater.*, 2016, **28**, 9408–9415.